Schweizerische Eidgenossenschaft
Confédération suisse
Confederazione Svizzera
Confederaziun svizra

Department of the Environment, Transport, Energy and Communication DETEC

Swiss Federal Office of Energy SFOE
Energy Research

Final report 28.03.2018

SMARTCAT

Development of a “smart concept” for biogas upgrade by continuous CO_2 methanation

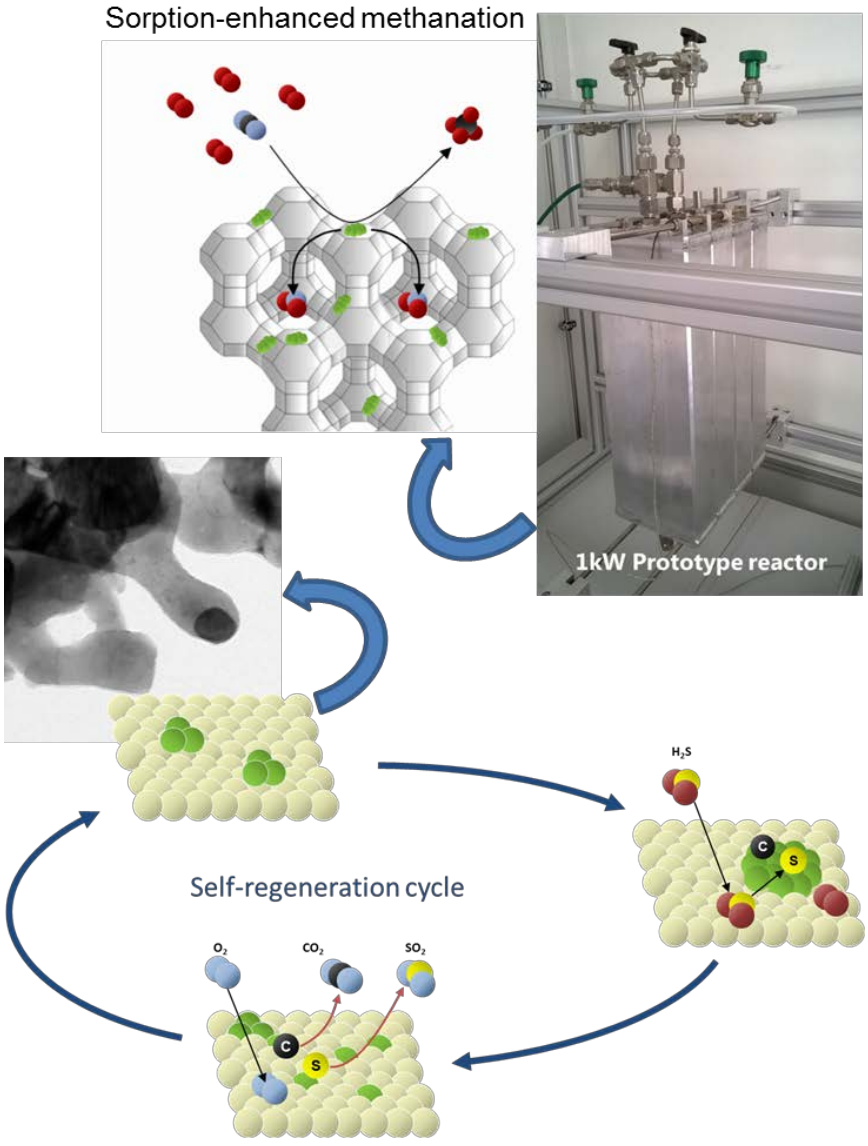

Date: 27.03.2018
Town: Winterthur

Publisher:
Swiss Federal Office of Energy SFOE
Bioenergy Research Programme
CH-3003 Bern
www.bfe.admin.ch

Co-financed by:
SVGW - Schweizerischer Verein des Gas- und Wasserfaches
Grütlistrasse 44, CH-8027 Zürich

Authors:
Renaud Delmelle, ZHAW, renaud.delmelle@zhaw.ch
Andreas Borgschulte, EMPA, andreas.borgschulte@empa.ch
Andre Heel, ZHAW, andre.heel@zhaw.ch

SFOE head of domain: Sandra Hermle, sandra.hermle@bfe.admin.ch
SFOE programme manager: Sandra Hermle, sandra.hermle@bfe.admin.ch
SFOE contract number: SI/501130-01

Swiss Federal Office of Energy SFOE
Mühlestrasse 4, CH-3063 Ittigen; postal address: CH-3003 Bern
Phone +41 58 462 56 11 · Fax +41 58 463 25 00 · contact@bfe.admin.ch · www.bfe.admin.ch

Zusammenfassung

Die Produktion von erneuerbaren Energieträgern hat in der Schweiz stark zugenommen. Die Schweizer Gaswirtschaft will – weil der Anteil an inländischem Biogas erst 1% beträgt – dessen Einspeisung markant erhöhen und bis 2030 einen Anteil von 30% im Wärmemarkt erreichen.

Da Biogas zu ca. 50% aus Methan (CH_4) besteht, müssen die restlichen Komponenten, CO_2 und H_2O, vor der Einspeisung in das Gasnetz abgetrennt werden. Das Projekt SMARTCAT zielt daher auf ein Biogas-Upgrade ab: Zwei neuartige Katalysator- & Reaktorkonzepte wurden für die anspruchsvolle, katalytische CO_2 Methanisierung aus Biogasen entwickelt. Mittels innovativer Materialkonzepte konnte einerseits katalytischen und mikrostrukturellen Degradationserscheinungen durch hohe Temperaturen bzw. Katalysatorgifte und anderseits dem geringen Wirkungsgrad hinsichtlich der CH_4 Ausbeute und der Ressourceninsuffizienz entgegengewirkt werden.

Ein sich unter dynamischen Betriebsbedingungen selbstregenerierender Katalysator ermöglicht es, die katalytisch aktive Phase nanodispers aus der Struktur auszulösen, aber sie auch reversibel wieder einzubauen. Durch gezieltes Materialdesign erreicht der neuartige Katalysator mit nur 2.5 Gew.% Nickel einen Methananteil von 80% bei 450-500 °C. Zur reversiblen Regeneration benötigt es noch 650 °C, weil die Nickeldiffusion mit sinkender Temperatur zu stark gehemmt ist. Jedoch konnte nach multipler Regeneration gezeigt werden, dass die sich die Mikrostruktur wieder optimal und feindispers aufbaut und so längere Standzeiten erlaubt und der Degradation entgegenwirkt.

Zum anderen wurde ein sorptionsbasierte CO_2 Methanisierung eingesetzt, welche bei 300 °C eine vollständige CO_2 Umsetzung zu Methan erreicht. Am Reaktorausgang liegt ohne nachgeschaltete Gasseparation ein trockener und zu 100% aus CH_4 bestehender Produktstrom vor, der keine praktisch relevanten Anteile an CO_2, CO oder Feuchtigkeit aufweist.

Um den technologischem Reifegrad (TRL) zu erhöhen, wurde ein 1 kW Prototyp konstruiert und erbaut, an dem die prozessrelevanten Betriebsparameter für die Methanisierung und die diffusionslimitierte Regeneration ermittelt wurden. Das modulare Reaktorkonzept ist damit für einen Technologietransfer in eine Demonstrationsanlage bereit.

Résumé

La part des carburants renouvelables dans le paysage énergétique suisse progresse d'année en année. L'objectif de l'industrie gazière suisse est d'augmenter cette part de 1% en 2018 jusqu'à 30% en 2030 sur le marché des énergies de chauffage. Le projet SMARTCAT est articulé autour du thème de la valorisation du biogaz, avec pour objet d'étude deux concepts innovants pour la catalyse de la méthanation du CO_2. D'une part, ces concepts apportent des solutions aux phénomènes de dégradation des catalyseurs actuels: dégradation catalytique et microstructurale, contamination. D'autre part, ils améliorent le rendement en méthane du procédé.

Le premier de ces concepts est l'auto-régénération d'un catalyseur par oxydoréduction. Ce résultat est atteint en utilisant un support de type pérovskite capable d'exsolver et de réincorporer de manière réversible une distribution de nanoparticules de nickel. Ici, la preuve expérimentale de ce concept est faite avec un catalyseur contenant moins de 2.5% de nickel et opérant dans l'intervalle 450-500°C avec un rendement en méthane d'environ 80%. La température de fonctionnement a ainsi été réduite de 450°C par rapport à notre composition de départ. Toutefois, une température de 650°C est nécessaire pour activer la diffusion des cations pour la phase de réincorporation. Celle-ci se fait sur des durées de l'ordre de l'heure, ce qui permet d'augmenter la durée de vie du catalyseur et de lutter contre sa dégradation microstructurale.

Le deuxième concept consiste en l'amélioration du rendement en méthane de la réaction de Sabatier au moyen de l'adsorption de l'eau produite par cette dernière par un support hydrophile. Des zéolites ont été utilisées à cet effet, toujours avec du nickel comme élément actif. Le rendement en méthane (sec) a été poussé jusque 100% à 300°C, sans produit non désiré, et donc sans la nécessité d'une étape ultérieure de séparation en phase gazeuse. Nous avons intensifié le procédé en portant sa puissance à 1 kW. Ses paramètres principaux - dimensionnement d'un démonstrateur de type modulaire, cinétique (limitante) d'évolution de l'eau pour la méthanisation et le séchage des zéolites - ont été optimisés.

Summary

Renewable fuels play a key role in the Swiss energy landscape. While the amount of renewable biogas is just 1% as of 2018, the Swiss gas industry aims to increase this amount up to 30% in the heating market until 2030. The SMARTCAT project focusses on a biogas upgrade: two novel catalytic CO_2 methanation concepts are explored and established to provide solutions to typical degadation mechanisms, that is catalytic and microstructural degradation from operation temperature and typical poisons as well as an insufficient methane yield.

At first, a perovskite-type catalyst whose host matrix is capable of reversibly exsolve and reincorporate the catalytic active metal nanostructures when redox cycled. The proof-of-concept is given here and it is shown that such concept can be operated at less than 2.5 wt% of nickel at 450-500 °C with a methane yield of about 80% under stoichiometric conditions. This is about 450 °C lower than initial operation temperature of the very first material composition. Redox cycling needs to take place at 650°C, keeping in mind, that lower temperatures limit the cation diffusion in the ceramic host. However, the microstructure is fully recovered on an hourly time level, allowing an extended lifetime of catalysts and counteract microstructure degradation.

Secondly, improvement of the methanation efficiency is tackled by sorption enhanced catalysis, providing a full CO_2 conversion to methane: A yield of 100% of dry CH_4 is reached without any practical relevant amounts of CO_2, CO, or humidity at temperatures as low as 300°C and that without any additional separation steps. To shift the technology readiness level from proof-of-concept to a technology relevant level, a 1 kW demonstrator was constructed and operated to receive operation relevant process parameters on the methanation and diffusion controlled drying. A modular concept is established which solved this, ready for transfer into a demonstration plant.

Appendix

Scientific project output: peer-reviewed publications in frame of the SMARTCAT project:

1) Burnat, Kontic, Holzer, Steiger, Ferri, Heel. Smart material concept: reversible microstructural self-regeneration for catalytic applications. *Journal of Materials Chemistry A*, 2016. **4**(30): p. 11939-11948.

2) Borgschulte, Delmelle, Duarte, Heel, Boillat, Lehmann. Water distribution in a sorption enhanced methanation reactor by time resolved neutron imaging. *Physical Chemistry Chemical Physics*, 2016, 18: p. 17217-17223.

3) Delmelle, Duarte, Franken, Burnat, Holzer, Borgschulte, Heel. Development of improved nickel catalysts for sorption enhanced CO2 methanation. *International Journal of Hydrogen Energy*, 2016, 41(44): p. 20185-20191.

4) Steiger, Delmelle, Foppiano, Holzer, Heel, Nachtegaal, Kröcher, Ferri. Structural Reversibility and Nickel Particle stability in Lanthanum Iron Nickel Perovskite-Type Catalysts. *ChemSusChem*, 2017, 10, 2505 – 2517.

5) Delmelle, Remhof, Heel, Proost, Borgschulte. Deactivation of a sorption enhanced methanation catalyst under operation conditions. Catal. Sci. Technol. under review (2018).

6) Borgschulte, Delmelle, Terreni, Heel. Concept, materials, design, and realization of a 1kW Sorption enhanced methanation reactor. In preparation.

References:

[1] C. Graves, S.D. Ebbesen, M. Mogensen and K. S. Lackner, *Renewable Sus. Energy Rev.* 15 (2011) 1-23.

[2] D. Papargyriou and J.T.S. Irvine, *Solid State Ionics* 288 (2016) 120-123.

[3] M.A. Peña and J.L.G. Fierro, *Chem. Rev.* 101 (2001), 1981-2017.

[4] D. Burnat, R. Kontic, L. Holzer, P. Steiger, D. Ferri and A. Heel, *J. Mater. Chem. A* 4 (2016) 11939-11948.

[5] A. Borgschulte, N. Gallandat, B. Probst, R. Suter, E. Callini, D. Ferri, Y. Arroyo, R. Erni, H. Geerlings and A. Züttel, *Phys. Chem. Chem. Phys.* 15 (2013) 9620-9625.

[6] M.A.A. Aziz, A.A. Jalil, S. Triwahyono and A. Ahmad, *Green Chem.* 17 (2015) 2647-2663.

[7] B. Miao, S.S.K. Ma, X. Wang, H. Su and S.H. Chan, *Catal. Sci. Technol.* 6 (2016) 4048-4058.

[8] S. Rönsch, J. Schneider, S. Matthischke, M. Schlüter, M. Götz, J. Lefebvre, P. Prabhakaran and S. Bajohr, *Fuel* 166 (2016) 276-296.

[9] M. Götz, J. Lefebvre, F. Mörs, A. McDaniel Koch, F. Graf, S. Bajohr, R. Reimert and T. Kolb, *Renewable Energy* 85 (2016) 1371-1390.

[10] M.D. Argyle and C.H. Bartholomew, *Catalysts* 5 (2015) 145-269.

[11] D.M. Bibby, R.F. Howe and G.D. McLellan, *Appl. Catal. A* 93 (1992) 1-34.

[12] G. Zhang, T. Sun, J. Peng, S. Wang and S. Wang, *Appl. Catal. A* 462-463 (2013) 75-81.

[13] C.H. Bartholomew, *Appl. Catal. A* 212 (2001) 17-60.

[14] S. Szabo and I. Bakos, *Corr. Rev.* 20 (2002) 95-104.

[15] B. Iwanschitz, L. Holzer, A. Mai and M. Schütze, *Solid State Ionics* 211 (2012) 69-73.

[16] J.A. Moulijn, A.E van Diepen and F. Katepijn, *Appl. Catal.* A 212 (2001) 3-16.

[17] P. Steiger, R. Delmelle, D. Foppiano, L. Holzer, A. Heel, M. Nachtengaal, O. Kröcher and D. Ferri, *ChemSusChem* 10 (2017) 2505-2517.

[18] M.A.A. Aziz, A.A. Jalil, S. Triwahyono, R.R. Mukti, Y.H. Taufiq-Yap and M.R. Sazegar, *Appl. Catal. B* 147 (2014) 359-368.

[19] R. Delmelle, R.B. Duarte, T. Franken, D. Burnat, L. Holzer, A. Borgschulte and A. Heel, *Int. J. Hydrogen Energy* 41 (2016) 20185-20191.

[20] C.H. Bartholomew, *Appl. Catal. A* 212 (2001) 17-60.

[21] A. Borgschulte, E. Callini, N. Stadie, Y. Arroyo, M.D. Rossell, R. Erni, H. Geerlings, A. Züttel and D. Ferri, *Catal. Sci. Technol.* 5 (2015) 4613-4621.

[22] S. Walspurger, G.D. Elzinga, J.W Dijkstra, M. Sarić and W.G. Haije, *Chem. Eng. J.* 242 (2014) 379-386.

[23] A. Borgschulte, R. Delmelle, R.B. Duarte, A. Heel, P. Boillat and E. Lehmann, *Phys. Chem. Chem. Phys.* 18 (2016) 17217-17223.

Contents

List of abbreviations

PtG	Power-to-gas
SOFC	Solid oxide fuel cells
LTA	Linde type A
FAU	Faujasite
GHSV	Gas hourly space velocity
LST	Perovskites of generic formula $La_xSr_{1-1.5x}Ti_{1-y}Ni_yO_{3-\delta}$
LNF	Perovskites of generic formula $LaFe_{1-x}Ni_xO_{3-\delta}$
SSA	Specific surface area
XRD	X-ray diffraction
TCD	Thermal conductivity detector
TPR	Temperature programmed reduction
TPO	Temperature programmed oxidation
XAS	X-ray absorption spectroscopy
DRIFTS	Diffuse reflectance infrared Fourier transform spectroscopy

Project Background

The Swiss government has signed the Paris Climate Agreement which implies that various measures need to be implemented in order to reach the target of a 50 % reduction in CO_2 emissions in Switzerland by 2030 compared to the value for 1990. Therefore, renewable energy carrier from biogenic ressources play a key role in the Swiss energy landscape. Typical biogases contain only of about 50-60% of methane (CH_4), while the residual components are mainly value-free CO_2, humidity and unfortunately catalyst poisons, such as sulfur components. However, a so-called biogas upgrade would be able to increase the methane yield by converting the residual CO_2 with renewable hydrogen via a catalyst to methane. Such a biogas upgrade will increase process efficiency and boost resources sufficiency.

Project Objectives

The objective of the project is the development and demonstration of a new concept for a continuously operated CO_2 methanation reactor. On base of novel and innovative concept - a self-regenerating sorption catalyst (SMARTCAT) - it has to be demonstrated how residual CO_2 from biogas plants can be converted highly efficient to methane. The methane should be of such a quality, directly after conversion and without any additional gas separation, that it can be injected into the existing natural gas grid. More precisely, it is aimed for a practically CO, CO_2 and water-free CH_4. By this, an economical interesting efficiency as well as a better resources sufficiency is gained, making this kind of renewable energy carrier more competitive.

For a fast and reliable technology transfer to industry, it is aimed for the installation a 1 kW reactor with the necessary studies on suitable reactor design, construction and operation conditions such as space velocities, operating temperature and temperature distribution, regeneration conditions, energy balance and resulting gas quality. Finally, a subtask aims at the demonstration of applicability of research results for power-to-gas application on a semi-industrial level, with a focus on long-term stability of catalysts, cycling management, and self-regeneration.

1. Introduction

The conversion of CO_2 with hydrogen into methane is an important step in the PtG concept for the seasonal storage of renewable energy [1]. In this project, we explored two novel catalyst concepts for CO_2 methanation from biogas sources, using Ni as active element and introducing novel properties through the use of specific support materials.

The first concept is a self-regenerating catalyst, where the oxide host support exhibits a perovskite crystal structure. When exposed to a reducing atmosphere with a low oxygen partial pressure, perovskites are able to exsolve metallic elements out of their structure [2], which results in finely distributed nanoparticles. Such materials are used for diverse catalytic processes [3], e.g. pollution abatement, photocatalysis and hydrogenation reactions. We recently showed that, under certain conditions, e.g. high oxygen partial pressure, the exsolution is reversible [4]. Repetitive redox cycles allow the metallic phase to reversibly enter and leave the parent perovskite structure. If the redox conditions are close enough to the operation temperature of the nanoparticles for a given catalytic reaction, this provides the answer to deactivation phenomena like coking and sulfur poisoning. This novel concept offers a microstructural as well as catalytic regeneration under operation conditions. We demonstrated this principle in earlier studies for SOFC anode materials at high temperatures of about 900 - 1200 °C [4], which is too high compared to methanation catalysts. Here, the challenge was the implementation of this concept to milder temperatures. We identified a perovskite composition suitable for application as a methanation catalyst. The catalytic activity is comparable to classic Ni-based catalysts, although our catalyst contains significantly less nickel. More importantly, we showed that this composition exhibits reversible Ni exsolution under relatively mild redox cycling conditions and is thus suitable for in-situ self-regeneration. However, redox cycling and screening under SO_2 containing atmospheres shows that the reincorporation of Ni in the perovskite structure is hindered by Sulphur. The oxidation step is the most critical step in real-life gas environments.

The second concept focuses on the catalyst performance and product quality rather than resistance to poisoning. We recently demonstrated the increase in the conversion yield of CO_2 methanation via the so-called sorption enhanced catalysis [5]. The catalyst for sorption enhanced methanation of CO_2 is nickel nanoparticles dispersed within the pores of a zeolite (here, LTA and FAU framework types were considered), which is known to readily absorb large quantities of water. By making use of Le Châtelier's principle, it is possible to push the methane yield of the Sabatier reaction to 100%. In the context of this project, our aim was the development of a 1kW Sorption enhanced methanation reactor. For a practical realization of a large scale reactor, critical parameters must be determined to optimize the geometry of the design. An important difference to fixed bed reactors without sorption functions is that the amount of catalyst is significantly higher in sorption reactors, as one product (water) remains in the bed. The reactor performance is thus linked to the absolute water adsorption capacity. However, this requires a careful definition of the dimensions of the reactor aligned to the planned operation conditions. On the other hand, the properties of the sorption catalyst predefine the performance of a reactor, and the reactor design has to be aligned to the material properties. One important outcome of this research project is the classification of the various parameters: catalytic activity of the material is defined on the atomistic scale by the reaction mechanism, but the local concentration depends on the state of the catalyst (mainly the water content), and on the mass transport of hydrogen, carbon dioxide, and subsequent reaction product taking place on the mesoscopic and macroscopic scale. Changes of the catalytic activity induced by poisoning are exclusively defined at the microscopic level, while heat transport is controlled by mesoscopic and macroscopic parameters. Another important outcome is the assessment of the catalyst long-term properties, which turns out to be excellent, despite a progressive decrease of the water evolution kinetics attributed to pore blocking in the zeolite structure.

2. The Sabatier reaction: Fundamentals and current catalysts

The fundamental of the CO_2 methanation process is the Sabatier reaction, an established reaction known since more than 100 years:

$$4H_2 + CO_2 \rightarrow 2H_2O + CH_4, \ \Delta H = -165 \frac{kJ}{mol} \quad (1)$$

The strongly exothermic heat of formation allows theoretically a thermodynamically high reaction yield in particular at low temperatures. However, this is practically not found, because the Sabatier reaction is a complex surface reaction, which is kinetically limited. This kinetic barrier can be overcome using catalysts. Commercial catalysts in fixed bed reactors reach conversion rates which are typically in the range (70 - 90%) [6], with corresponding operation temperatures being in the range (200 - 400°C). One should note that a CO_2 conversion of 98% results in a methane purity of only about 90%. The remaining 10% consist of mainly unreacted H_2 and CO_2 as well as CO.

Despite the apparent simplicity of reaction (1), in total eight electrons and hydrogens are transferred, leading to a complex reaction mechanism:

$$\boldsymbol{CO_2 + 4H_2} \rightarrow$$

$$\rightarrow CO_2^* + 8H^* \quad (2a)$$

$$(+OH^-) \rightarrow HCO_3^- + 8H^* \quad (2b)$$

$$\rightarrow COOH^* + 7H^* \quad (2c)$$

$$\rightarrow CO^* + H_2O^* + 6H^* \quad (2d)$$

$$\rightarrow C^* + H_2O^* + H_2O^* + 4H^* \quad (2e)$$

$$\rightarrow CH_n^* + 2H_2O^{(*)\uparrow} + (4-n)H^* \ (2f)$$

$$\rightarrow \boldsymbol{CH_4 + 2H_2O}$$

Due to the high barrier of the various steps in the gas phase, the reaction takes place on catalytic surfaces only. The asterisk denotes species adsorbed to this surface. Reactions (2a)-(2f) refer to the reaction taking place on Ni particles supported by oxide supports. The reaction steps may be described as hydrogen dissociation and CO_2 adsorption (2a), CO_2-activation (2a, 2b), hydrogen addition (2c, 2f) and water formation (2d, 2e). Each of these individual reactions steps may be rate-limiting, as the slowest step determines the overall reaction kinetics. If the reaction is in dynamic equilibrium, the consequence of eliminating the barrier of the rate-limiting step is that a new rate-limiting step establishes. The optimal catalyst has thus multi-functional properties.

Established catalysts for CO_2 methanation are based on Ni, or Ni-like metals such as Ru, which catalyze hydrogen dissociation, water formation and the hydrogenation of carbon and carbon oxides [7]. Although these metals are able to activate CO_2, the adsorption of CO_2 on Ni is relatively small and thus the overall rate for CO_2 activation moderate. To account for this function, the metal particles are supported on oxides, which adsorb CO_2 very well. Hydroxide ions react with the CO_2 forming carbonate species, which is transported to the Ni-oxide interface. On the Ni surface, reduction to COOH, CO, and carbon take place. The last steps are the additions of hydrogen to CH_n forming methane.

From a practical point of view, even if the activity of current catalysts is fairly good, it would be highly valuable to further increase the yield of conversion of CO_2 from industry (e.g. to avoid gas purification). The interest of building more robust catalyst against poisons from said sources is trivial. These are the two main focuses of the present research project. An early idea was to unify both concepts. However, the temperature conditions turned out to be too different, so that we decided to continue the development of both catalysts as different systems.

3. Self-regenerating catalysts for CO_2 methanation

3.1 Self-regeneration concept

As stated above, the Sabatier reaction is known for a long time and the related processes are the object of continuous development efforts. Established methanation processes [8,9] involve fixed-bed, fluidised-bed and three-phase reactors with classic metal-support catalyst systems (e.g. Ni on alumina). At a purely fundamental level, ruthenium competes with nickel, but its price pushes it out of the game for commercial applications. Although other elements are still considered (e.g. Fe, Co, and Mo), nickel remains the most suitable active metal and by far the most widely used in commercial applications, when considering activity, selectivity and price [6,8]. However, similar to most elements in group 8-10 considered as active metals for methanation, nickel is facing durability issues that simultaneously affect the process performance, cost and environmental impact. Depending on the process considered and on the methanation conditions - GHSV, temperature, pressure, stoichiometry and reactant purity - different deactivation mechanisms can potentially occur: catalytic degradation (poisoning) [10], fouling (coated by coking) [11], thermal degradation [12], mechanical degradation (attrition, crushing) [13], corrosion (leaching) [14] and microstructural degradation (particle growth) [15]. Despite their differences, these mechanisms all affect the concentration of active sites on the catalyst surface, in turn lowering the apparent rate constant for methanation. The development of effective solutions to these deactivation issues is a crucial research topic for future applications [16]. This is particularly true regarding sulfur poisoning, since, on the one hand, sulfur is known to strongly adsorb on Ni surfaces and even form sulphides, in turn dramatically affecting the catalyst activity, even at ppm level. Specific solutions exist against each of these issues, but an elegant solution should be more general. Among the deactivation mechanisms described above, all of them can be fought by our self-regeneration concept. The latter implies the use of perovskites as supports for the active element. Perovskites are metal oxides of generic formula $ABO_{3-\delta}$ (anion nonstoichiometry δ is common in such crystals), with the A cation having a larger size than B [3]. Here, we consider the case where the B site is partly occupied by the catalytic active element, yielding the formula $AB_{1-x}M_xO_{3-\delta}$, where M is the catalytic active element. Nickel can be exsolved this way from the B site [2], but this does not mean that the B site is only filled with element M. If this was the case, the structure would irreversibly collapse towards the pure elements/oxides under reducing conditions. If the B site is mainly filled with a “backbone” element (i.e. which is not preferentially exsolved over M, which has an atomic radius as close as possible to M and which is as cheap as possible), specific compositions allow such perovskites to reversibly exsolve metallic elements according to the following reaction [4]:

$$AB_{1-x}M_xO_{3-\delta} \overset{Redox}{\longleftrightarrow} AB_{1-x}M_{x-\varphi}O_{3-\delta(\mathrm{lim})} + \varphi M + \frac{\delta(\mathrm{lim}) - \delta}{2} O_2 \quad (3)$$

x is the fraction of element M on the B site, φ is the extent of M reduction and $\delta(lim)$ is the maximum anion nonstoichiometry. Considering nickel as the active element and H_2 as the reducing gas, reaction (3) can be developed as follows:

$$\boldsymbol{AB_{1-x}Ni_xO_{3-\delta} + (\delta(\mathrm{lim}) - \delta)H_2} \rightarrow$$

$$\rightarrow AB_{1-x}Ni_xO_{3-\delta(lim)} + (\delta(\mathrm{lim}) - \delta)H_2O \quad (3a)$$

$$\rightarrow \boldsymbol{AB_{1-x}Ni_{x-\varphi}O_{3-\delta(lim)} + \varphi Ni + (\delta(\mathrm{lim}) - \delta)H_2O} \quad (3b)$$

The nonstoichiometry of oxygen in the perovskite lattice first evolves in reaction (3a), which in turn forces the structure to exsolve nickel atoms to compensate in reaction (3b). As mentioned above, if φ is too

high, reaction (3) will not be reversible anymore because there will not be enough left of the perovskite host lattice to sustain reincorporation of Ni atoms.

The self-regeneration concept is illustrated in Fig. 1. After long-term operation at moderate to high temperatures in sulfur-containing atmospheres - here, H_2S is represented, as a common catalyst poison present in biogas sources - deactivation can take place, e.g. in the form of contamination and particle growth. Periodic redox cycling of the catalyst-support couple allows getting rid of poisons like C and S (clean off) and restoring the particle size, and ultimately, the concentration of active sites.

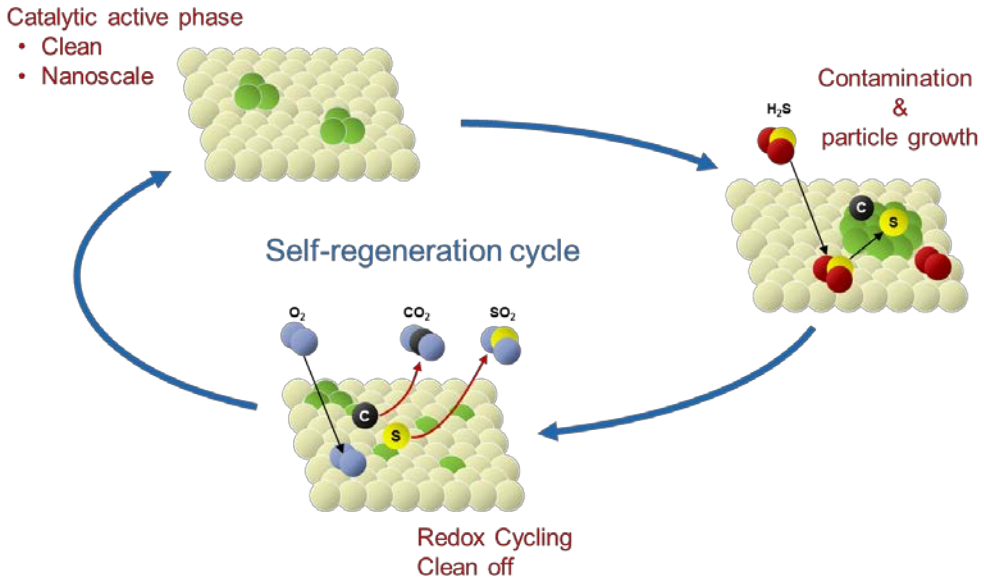

Figure 1: Concept of self-regeneration of a perovskite catalyst by redox cycling. The green atoms represent the active metal in the perovskite lattice.

3.2 Materials selection

Based on our experience of perovskites as catalyst materials, we derived a suitable composition range for application as a CO_2 methanation catalyst. As stated above, we initially demonstrated the self-regeneration principle using LSC-type perovskites [4] (i.e. A = La and Sr and B = Ti). Rather high temperatures up to 900°C are required if Ti is used on the B-site due to its low reducibility upon redox cycling. This is not a problem given the application they are aimed for, but such conditions are too harsh regarding CO_2 methanation. We tested other compositions with the aim of lowering the redox cycling temperatures. We opted for LNF-type perovskites (i.e. A = La and B = Fe) with Ni as the active element. We studied Ni concentrations on the B site in the range (0 - 20%). Above $x = 0.2$, the perovskite structure cannot be reversibly redox cycled [16]. Moreover, redox cycling temperatures required for obtaining phase pure crystals increase above this point, which can result in a decrease of the catalyst specific surface area (SSA).

$LaFe_{1-x}Ni_xO_{3-\delta}$ perovskites exhibit an orthorhombic structure for $x < 0.5$ ($LaFeO_{3-\delta}$ structure) and a rhombohedral structure for $x > 0.5$ ($LaNiO_{3-\delta}$ structure). So, over the range considered here, no phase transformation occurs. Metallic Ni is reversibly exsolved out of the orthorhombic perovskite lattice while the oxygen vacancies evolve at the same time. The Ni particle size was situated in the range of 5 - 50 nm from SEM and TEM imaging (see Figs. 2b and 2c), with an average size in the range of 20 - 30 nm

[17]. However, these numbers cannot be compared with crystallographic data, e.g. from XRD analysis. Characterization of these nanoparticles was found to be much more problematic than other nanoparticles of similar size (e.g. distributed on supports by classic methods like ion exchange or incipient wetness impregnation). As a matter of fact, the main Ni 111 and NiO 200 reflections are missing in Fig. 2a (see caption).

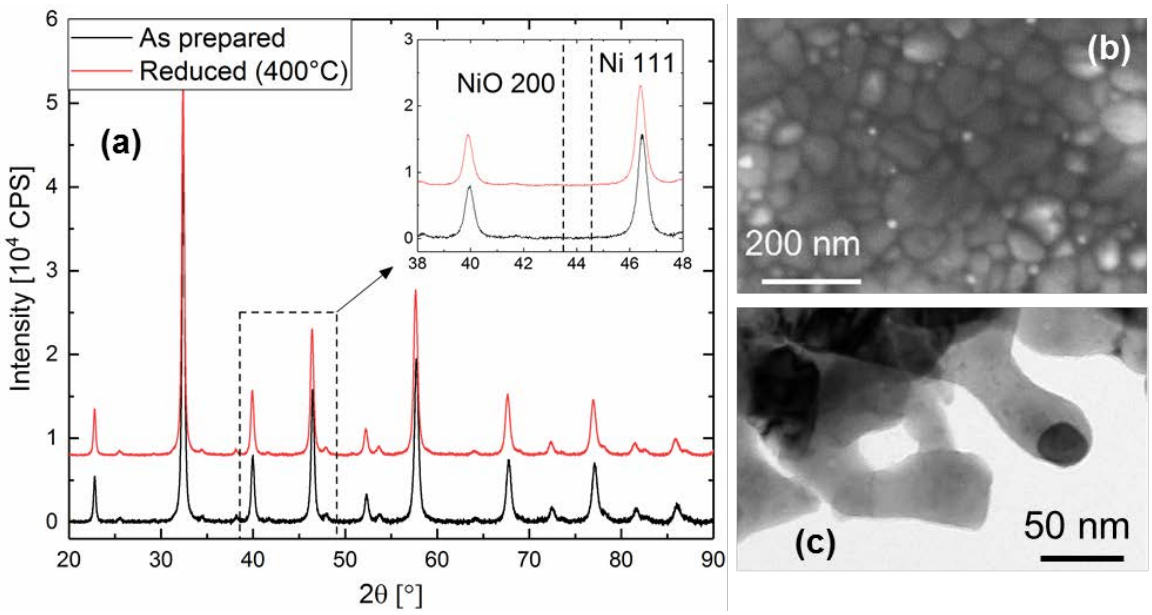

Figure 2: (a) XRD diffractograms of LNF specimens (x = 0.2) as prepared (using the citrate method, i.e. dissolution of nitrate precursors in H_2O together with citric acid, followed by drying and calcination) and after reduction (1h at 400°C). (b) SEM and (c) TEM images of the reduced specimens.

The reason for the absence of Ni reflections in the diffractograms of Fig. 2a is linked to the singularity of our materials in terms of catalyst-support interactions. Unlike the classic synthesis methods mentioned above - i.e. where the support is first synthesized, and as a second step, the active metal is distributed on it - the support already contains the active element after its synthesis. Upon reduction, it generates itself the active metal nanoparticles by exsolution, as explained above. The particles literally “grow” on the substrate atom by atom, comparatively to advanced thin film deposition techniques (sputtering, atomic layer deposition, etc.) where the film-substrate coherence is very strong in terms of crystallinity. This might result in nanoparticles either with strong crystalline relationship with the substrate or poor crystallinity. As will be shown below, we believe that this positively affects the activity of the catalysts.

3.3 Experimental proof and optimisation of the self-regeneration concept

The reduction of the catalysts after calcination was first studied with the help of TPR experiments. The latter consist in exposing a small amount of specimen to a continuous gas flow, imposing controlled heating and continuously monitoring the thermal conductivity of the gas mixture, composed of H_2 and a chemically neutral gas with significantly different thermal conductivity, here Ar. As H_2 is consumed by reduction of the specimen (see reaction (3a)), the TCD detector will detect changes in the thermal conductivity, which reflect the gas composition and the amount of hydrogen consumed. Fig. 3a shows such experiments performed on our LNF specimens. The peaks appearing in the range (150 - 300°C)

are clearly due to reduction and exsolution of Ni because the TCD signal is proportional to the Ni content in the specimens. At higher temperatures, the structure shows increasing instability with the Ni content, as shown by the sloped background in the range (400 - 700°C). Decomposition of the perovskite and reduction towards pure elements takes place above 700°C. From this dataset, it appears that the reduction temperature of the catalyst should be above 300°C. We chose 400°C as a safe reduction temperature, enabling for reproducible reduction profiles with reasonable kinetics (see also multiple redox cycles in Fig. 6). Higher temperatures are not wished because we also want to keep the active particle size as small as possible.

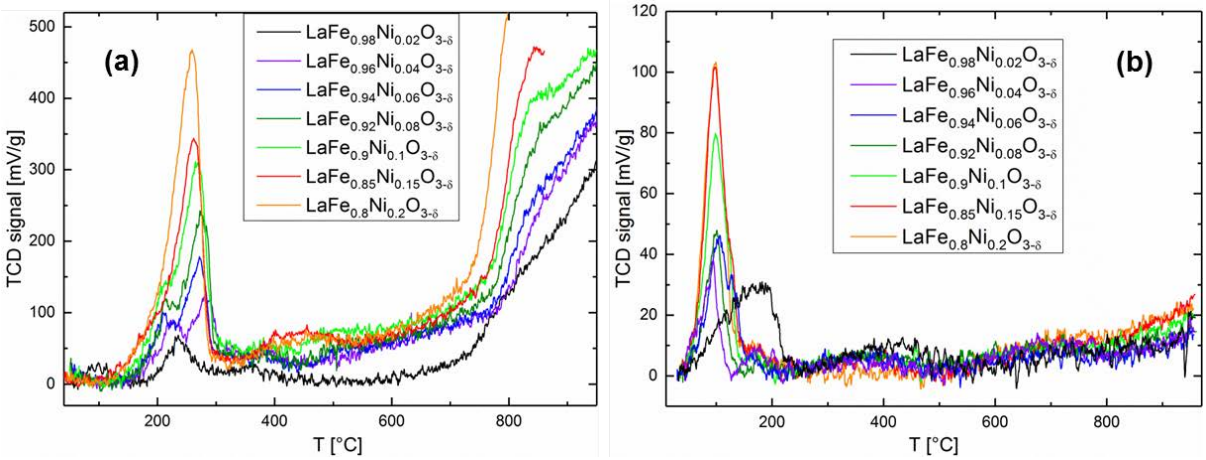

Figure 3: (a) TPR and (b) TPO experiments performed on LNF specimens with x = 0.02, 0.04, 0.06, 0.08, 0.1, 0.15 and 0.2; with a heating ramp of 5 K/min and respective gas compositions of 5% H_2 in Ar and 10% O_2 in He. Changes in TCD signal reflect hydrogen and oxygen consumption, respectively.

The same device can also be used to perform so-called TPO experiments on the reduced specimens, i.e. with O_2 as the reactive gas. This is not as evident as the TPR experiments because oxidation of the specimens - and more specifically, of the Ni nanoparticles - starts readily at room temperature. Early oxygen consumption is difficult to monitor because the experiment can only start after circulating the probing gas mixture. However, these experiments are of high interest as well, one should simply keep in mind that they are quantitatively less meaningful than the TPR experiments. Fig. 3b shows the TPO data of the same specimens as in Fig. 3a, after an in-situ pre-reduction step. Oxidation starts at lower temperatures than reduction. Here again, the proportionality with Ni content in the specimens shows that the O_2 consumption comes from reoxidation of nickel (even if this proportionality is less evident for the reasons explained above). Above 350°C, no significant O_2 consumption is further observed. This does not mean that reincorporation of Ni in the perovskite structure takes place below 350°C. In a parallel study, we showed by XAS spectroscopy that temperatures of at least 600°C are necessary in order to obtain full reincorporation of the nickel [17]. This can be indirectly proven by employing a very common method in catalysis: performing multiple TPR/TPO cycles and aiming to reproduce the TPR profile of the as-prepared specimen (see Fig. 6).

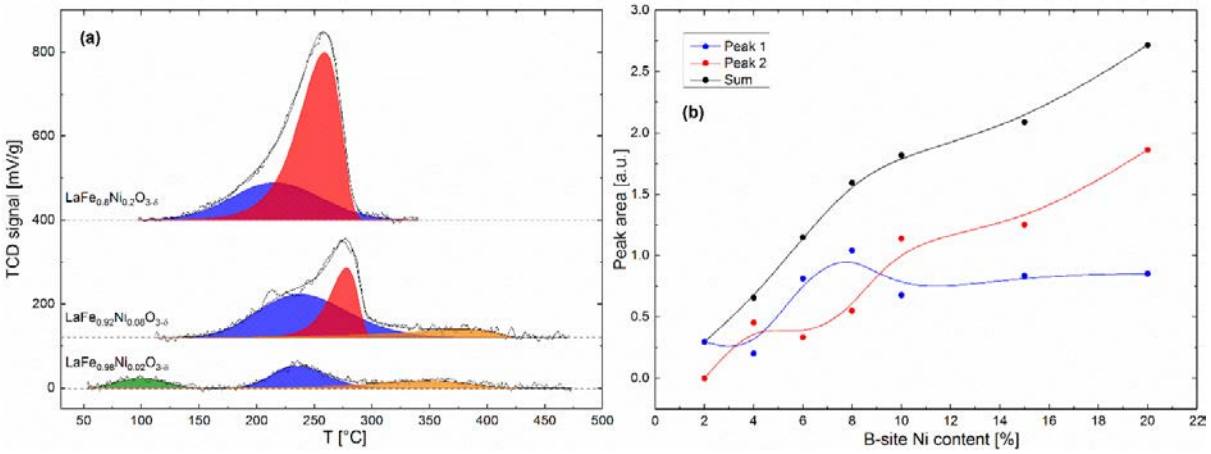

Figure 4: (a) Deconvolution of the TPR signals of Figure 3a for three perovskite compositions. In (b), the two main components of this deconvolution (blue and red peaks) are plotted against the B-site Ni content (x).

Deconvolution of the TPR profiles is shown in Fig. 4a. Besides the marginal green and orange components, which only appear in specimens with small Ni contents ($x < 0.1$), two main components were identified (red and blue peaks). As quantitatively shown in Fig. 4b, one of these peaks increases continuously until $x = 0.1$, while the other continuously increases even above this limit. $x = 0.1$ might be the point where bigger Ni particles are formed, with less crystalline coherency with the perovskite substrate. However, we don't have a definitive experimental proof for this theory. These observations will be further linked to the catalytic activity of the specimens (see next sections). The oxygen and hydrogen consumptions needed for the exsolution and reincorporation of nickel can be derived by integrating the peaks shown in Figs. 3 and 4. Fig. 5 shows that these consumptions are correlated. Chemically speaking, these trends make sense, from a qualitative point of view. However, as explained above, a direct quantitative assessment is not possible because of the uncertainty of the TPO measurements. For example, the large oxygen consumption observed when reoxidising $LaFe_{0.98}Ni_{0.02}O_{3-\delta}$ is difficult to interpret, and could be most logically attributed to an experimental artifact.

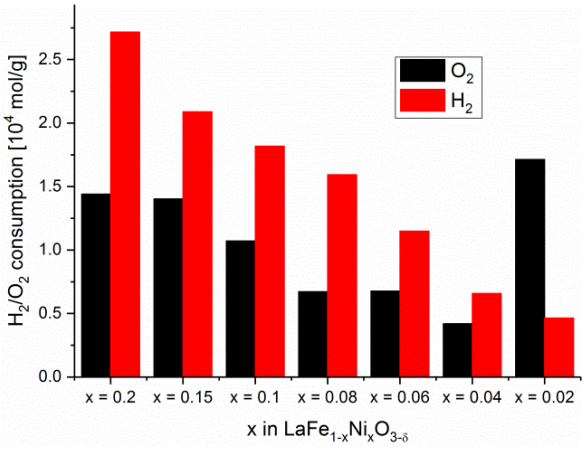

Figure 5: Oxygen (black) and hydrogen (red) consumptions recorded during TPR and TPO, as integrated from the curves shown in Figure 3.

Finally, once the redox cycling conditions are adjusted with the help of TPR/TPO data (Figs. 3-5), it is necessary to perform multiple redox cycling in order to prove the self-regeneration concept. The shape and surface of the TPR profiles provide information about the extent of preceding oxidation steps. The effect of different oxidation parameters is investigated in Fig. 6. First, Fig. 6a shows the effect of oxidation

temperature (gas composition and time are kept constant). Reoxidising at 400°C and 500°C gives TPR profiles which are significantly different from the as-prepared material, notably with the presence of unwanted shoulders at temperatures above and below the main peaks. We identified 600°C as the lower limit for activation of full Ni reincorporation (although practically, we don't reoxidise under 650°C to ensure acceptable reincorporation kinetics).

Secondly, the effects of oxidation time and gas composition (i.e. oxygen concentration in the oxidizing mixture) are shown in Fig. 6b. Independent of the latter parameters, Ni will not fully reincorporate into the perovskite structure if the temperature is too low. At 400°C, the Ni nanoparticles are oxidized, but reincorporation is not triggered. This comes in line with the conclusion drawn above from Fig. 6a.

Fig. 6c shows two consecutive redox cycles carried out under conditions ensuring full reincorporation. The same TPR profile is successfully reproduced three times in a row, which achieves to prove the self-regeneration concept by showing its durability. In the next section, these results will be put into perspective with the catalyst activity.

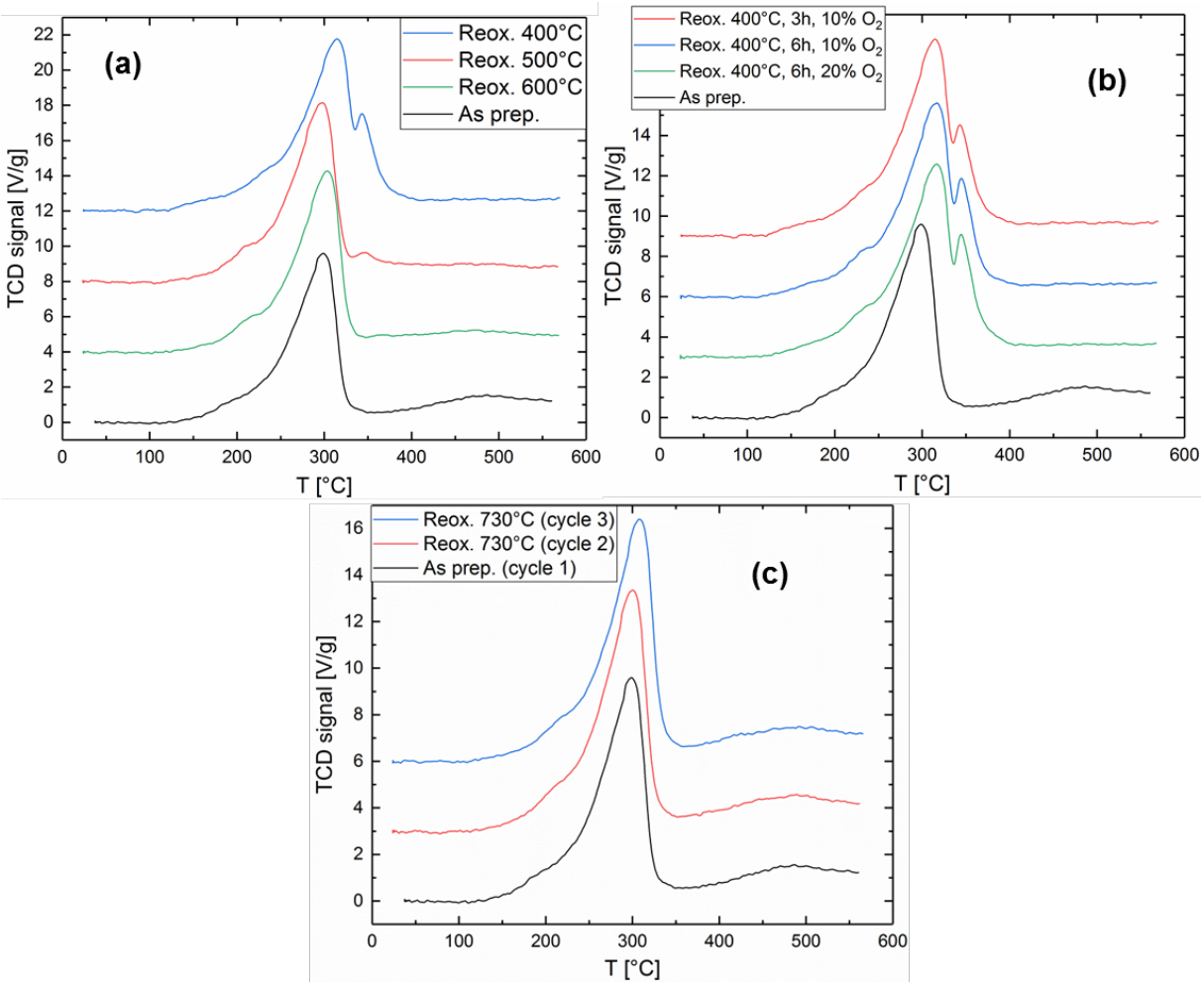

Figure 6: TPR curves performed on LNF specimens with x = 0.2 subjected to multiple redox cycles. The oxidation conditions prior to each TPR curve are the following, considering curves from bottom to top in each graph: (a) Calcined (2h in air at 700°C) - oxidised 3h in 10% O_2 at 600°C, 500°C and 400°C, (b) Calcined - oxidised at 400°C 6h in 20% O_2, 6h in 10% O_2 and 3h in 10% O_2, (c) Calcined - oxidized twice in a row 3h at 730°C in 10% O_2.

3.4 Catalytic activity, durability and poisoning

The catalytic activity of our perovskite specimens was studied by in-situ Raman spectroscopy. Gas flows were monitored by a multi-probe setup before and after the reaction, allowing for calibration of the gas composition. The latter was set to the Sabatier stoichiometry (4:1 H_2 to CO_2 ratio according to reaction (1)) with a hydrogen excess of 5%. Stepwise heating of the specimens was applied, with a waiting time of about 15 min for each temperature step in order to ensure for a good accuracy of the derivation of the methane yield. A GHSV of 2691 h^{-1} was applied during screening. This order of magnitude is within industrial standards of similar processes. Fig. 7 shows a typical screening experiment, here performed on a LNF of formula $LaFe_{0.9}Ni_{0.1}O_{3-\delta}$. Before screening, the specimen was exposed to pure H_2 at 400°C for 1 h. Then, the temperature was set to 450°C and CO_2 was introduced in to the system ("CO_2 in" in Figs. 7a and 7b). Fig. 7a confirms the good control and stability of the inlet gas flows and composition. Fig. 7b reveals that the catalyst selectivity is very good despite the observation of a few mol.% of carbon monoxide, especially at elevated temperatures, typical for such Ni supported catalysts. The catalyst responds relatively fast to temperature changes. The gas compositions during the temperature steps are stable and easily reproducible, either by screening with increasing or decreasing temperatures.

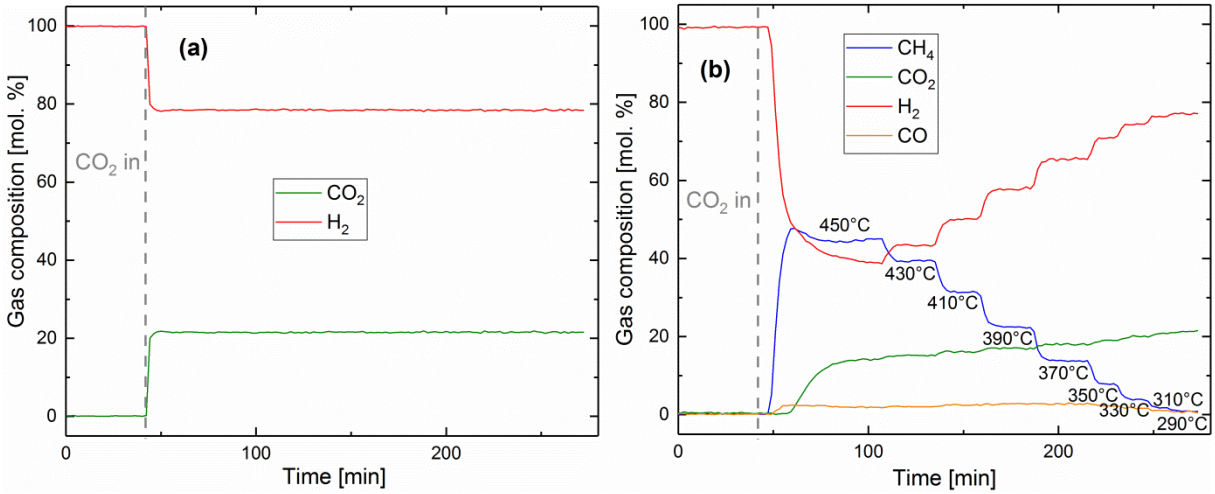

Figure 7: Gas concentrations at the reactor inlet (a) and outlet (b) during screening of a LNF specimen with x = 0.1, as determined by in-situ Raman spectroscopy. GHSV = 2691 h^{-1}. Reduction prior to screening was performed for 1h at 400°C with pure H_2.

Here, at 450°c, a methane yield of 70% is achieved with 2.4 wt.% Ni in the catalyst material. This value competes with existing catalysts, but the latter typically have much higher Ni loadings (in the range 5-20 wt.% [6]). This is a promising result, which could be explained by the particular substrate-catalyst crystallographic relationship in LNF perovskites (see 3.2). The latter could change the energetics of actives sites for methanation and improve the methane turnover frequency. This interpretation needs support from further fundamental investigations.

However, especially the low catalytic material amount offers a new option: Ni is a good catalyst, but not the best. It is more a trade-off between performance and costs. The extremely high dispersion provided by the perovskite based material developed here offers a cost competitive application of noble metal based elements, which in turn offers a much better performance at lower operation temperatures.

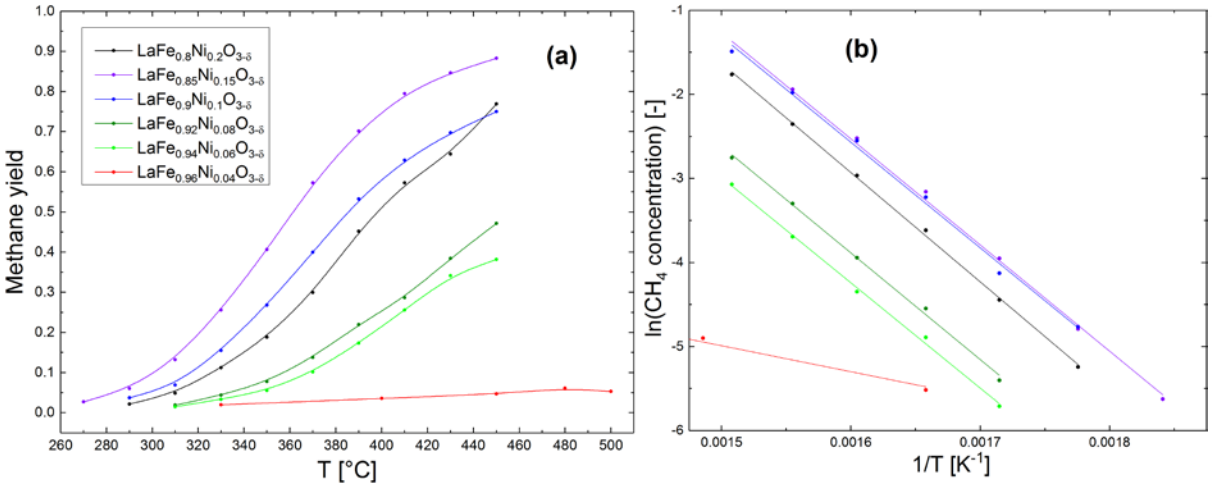

Figure 8: (a) Evolution of the methane yield as a function of the catalyst composition and (b) corresponding Arrhenius plots.

Fig. 8a displays the methane yield as a function of catalyst composition ($0.02 < x < 0.2$). The above observations are supported here: very small Ni loadings are still able to initiate the reaction, down to $x = 0.06$. Below this limit, the reaction mechanism itself changes, as indicated by the drastic change in the slope of the Arrhenius plots shown in Fig. 8b. From the latter, activation energies for the Sabatier reaction can be derived. The numbers are shown in Table 1. Activation energies of the Sabatier reaction on classic catalysts are typically around 100 kJ/mol [18], in agreement with our results. This quantitatively validates our in-situ approach and confirm the expected reaction pathway on the Ni nanoparticles.

Table 1: Activation energies for CO_2 methanation as a function of the Ni content on the B site in LNF perovskites.

***x* on B site**	**E_A [kJ/mol]**
4%	25.7
6%	104.2
8%	105.5
10%	104.5
15%	105
20%	108.1

The data from Fig. 8a show that, for $x < 0.1$, the catalyst activity does not further increase. Even if this dataset shows that $x = 0.15$ has the best activity, there is no trend anymore at this point. Coming back to the TPR data of Fig. 4, if only bigger particles are formed at this point, they would offer less active sites for catalysis and bringing more nickel into the perovskite lattice would be detrimental not only from a structural point of view, but also from the activity point of view.

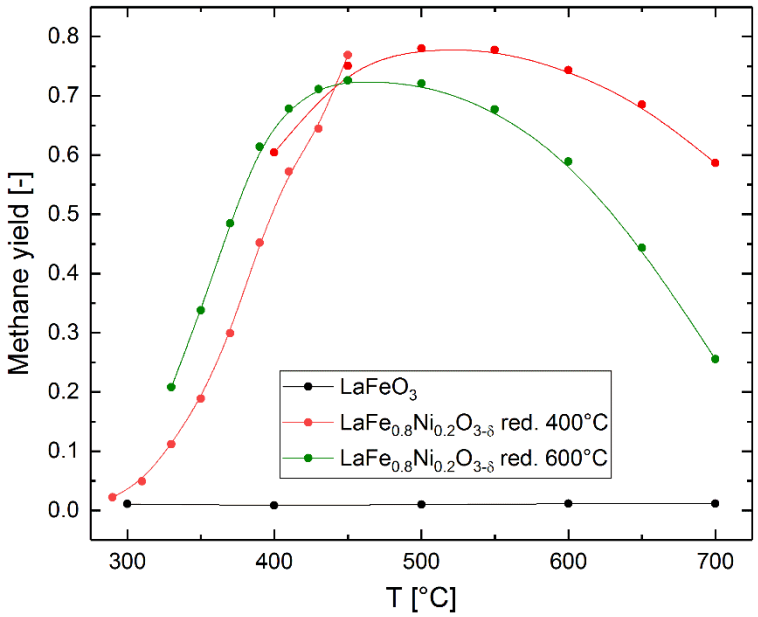

Figure 9: Evolution of the methane yield as a function of temperature of LNF specimens with x = 0.2. The two different red curves come from two different specimens.

Fig. 9 shows the methane yield over the whole temperature range up to the calcination temperature of the specimens (700°C). Around 450-500°C the activity reaches a maximum, and further decreases as the formation of carbon monoxide becomes favoured (i.e. here, the decrease of the methane yield means that the catalyst selectivity decreases, but not the overall activity). Screening of the blank specimen (x = 0) confirm the fact that Ni is indeed the only active species in our system. As explained above, we want to keep the reduction temperature as low as possible in order to avoid losing too much active surface area. Although harsher conditions are required for Ni reincorporation, reduction can be performed at milder temperatures. 400°C is a good value because the optimal activity is higher than specimens reduced at 600°C, even if the specimens reduced at 600°C exhibit better yields at lower temperatures. Again, our results confirm the fact that Ni reincorporation in to the host lattice is the most critical step in the self-regeneration process. Here, we must also point out a drawback of our perovskite catalysts: the optimal operation temperature is around 500°C, which about 100°C above the typical range of state-of-the-art materials [6].

These perovskites catalysts show excellent durability, as shown in Fig. 10. A catalyst exposed five times to alternating reducing and oxidising environments under operation conditions will retain its activity. No sign of catalytic or microstructural degradation was seen after operation on a week time scale.

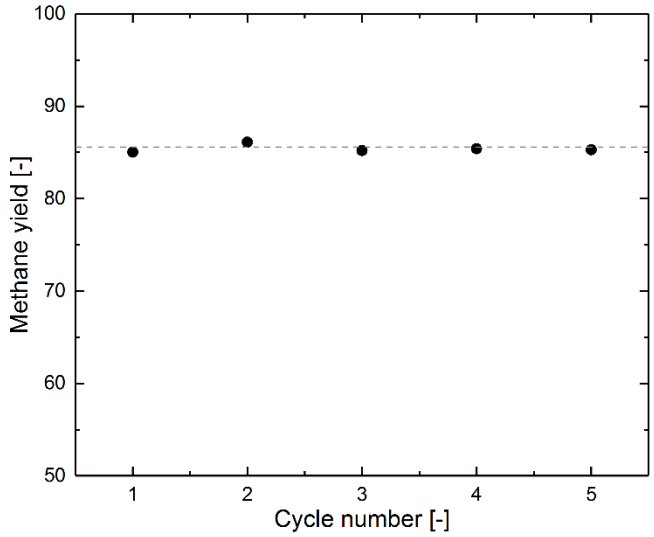

Figure 10: Methane yield as a function of cycle number for a LNF perovskite (x = 0.2) under operation conditions (atmosphere, 500°C) exposed five times to the following sequence: 30 min reduction in pure H_2, 20 min screening in H_2/CO_2 and 30 min oxidation in air.

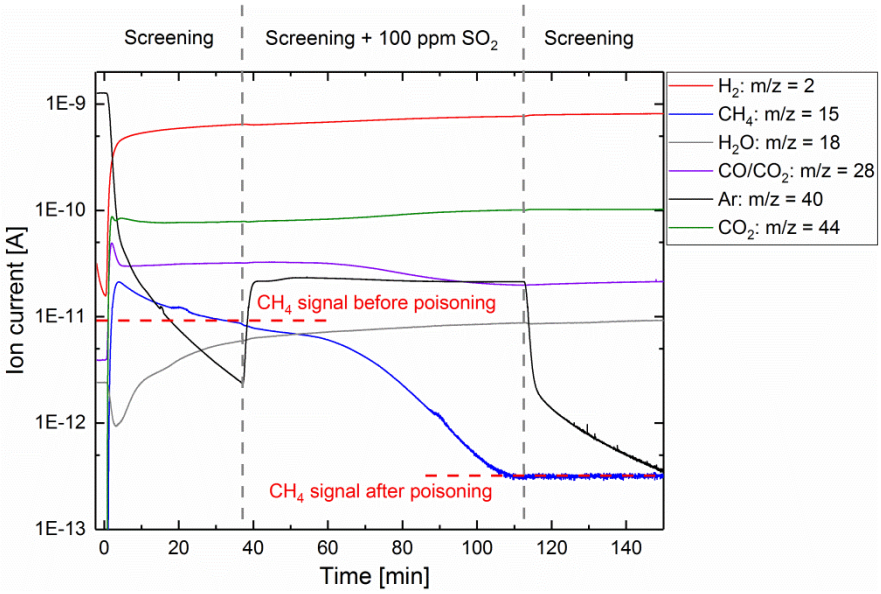

Figure 11: Mass spectrometry screening of a LNF perovskite with x = 0.2 under SO_2-containing atmosphere. SO_2 was provided in the form of a 1000 ppm containing Ar carrier gas. Although the SO_2 concentration is too small for detection, the carrier gas provides an indirect measurement.

However, in such high quality this is of course only true for sulfur-free gas mixtures. The perovskite catalysts were tested under SO_2-containing atmosphere (see Fig. 11). Like all Ni-based catalysts, these catalysts are very sensitive to sulfur containing gases. Deactivation takes place on an hour scale. Further attempts to regenerate the catalysts under the optimised conditions described in Section 3.3 failed to recover the catalyst activity. Pushing the oxidation temperature to 750°C did not lead to improvements. It still not clear whether adsorbed sulfurous species impede reincorporation or if bulk Ni sulphides are formed. Depending on the amount of sulfur in the input gas mixture, removal of sulfurous species prior to methanation seems to be a suitable technical solution until further studies clarified this effect. The author assume, that Ni underwent a transformation to Ni_3S_2, although some more recent

results give rise to an assumption that some so-far unknown adsorbed Ni-S intermediates could cover the surface, but this has to be proven in further studies.

One should realise that once a technical setup is used with sulfur components, it cannot be used anymore under sulfur-free conditions since the sulfur compositions are permanently poisoning the setups. However, this conclusion does not affect self-microstructural regeneration from other deactivations phenomena and will provide a substantial economic advantage in terms of keeping a high activity over an extended lifetime (see section 3.1). The consortium is currently exploring further strategies to counteract this sulfur problem, e.g. by alloying with additional sacrifice elements, keeping the sulfur from nickel away and replacement of Nickel by other elements less prone to poisoning.

4. Sorption-enhanced methanation: Towards 1kW system

4.1 Concept of sorption-enhanced methanation

Besides self-regeneration, sorption enhanced methanation, another new catalyst concept was studied in the context of this project to be comprised with the self-regeneration to reach a more competitive CO_2 methanation catalyst. The utilization of the Le Châtelier's principle by local absorption of the water at the reaction centers (see reaction (1)) improves the reaction kinetics and yield [5]. This is made possible by adding a water-affine sorbent to the catalyst, which is thus called sorption enhanced catalyst [18]. The corresponding concept is shown in Fig. 12. In contrast to sole catalysis, water adsorption is a bulk process, i.e., the reactor size scales with total amount of product, while in solely catalytic processes, the size scales with the flux (concept of "space velocity", turnover frequency). Furthermore, the sorption effect stops after saturation of the sorbent while the sorption catalyst simply behaves like any other conventional nickel based methanation catalyst. The regeneration, more precisely the removal of water, is thus an additional important step in the overall process. To avoid extra energy losses, it should take place at the same temperature as the reaction and thereby use the reaction heat to drive desorption of water. The plate reactor concept is aimed at enabling maximum heat exchange between cells running reaction and those being regenerated. Furthermore, it is easily up scalable. In a first step, we carefully studied the performance of a single cell. Important addressed questions are:

- What are optimal operation parameters for sorption enhanced catalysis?
- Is the design (shape, size) appropriate for optimal flow field and heat transport?
- Can the empirical parameters be modelled for future reactors running on different catalysts/ dimensions?

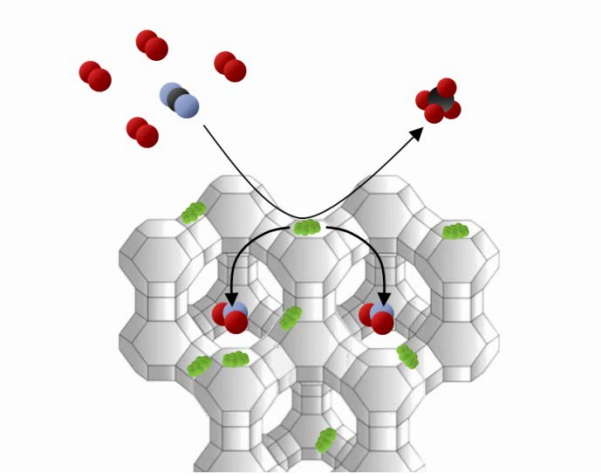

Figure 12: Molecular structure model of sorption enhanced CO_2 methanation over a nickel catalyst on zeolite. Red, blue, black and green spheres represent hydrogen, oxygen, carbon and nickel atoms, respectively.

Based on these considerations (see section 4.3), we developed a 1kW sorption enhanced methanation reactor as the final outcome of this project. Parallel to the works on the reactor design, we optimized the sorption catalyst. We focused on the following tasks:

- Catalytic activity: as high as possible conversion rate of CO2 to methane without side products such as CO and determination of optimal operation parameters (temperature, flows, pressure).
- High water sorption capacity and determination of optimal operation parameters (temperature, flows, pressure).
- Estimation of long-term stability of the catalysts with particular focus on degradation phenomena such as coking and poisoning by sulfur compounds.
- Optimization of regeneration process (drying): temperature, flows, pressure.

These materials properties are discussed in the next section.

4.2 Materials requirements

4.2.1 Reaction mechanism

Coming back to reaction (2), an important difference between the reduction step (2c) and the subsequent steps to CO (2d) and C (2e) is that the reduction is associative, i.e., only hydrogen is added to the molecule, while in (2d) and (2e) the addition of hydrogen leads to a dissociation of the molecule into water and CO and C, respectively. Water is a polar molecule, which adsorbs strongly to polar surfaces such as the oxide surface.

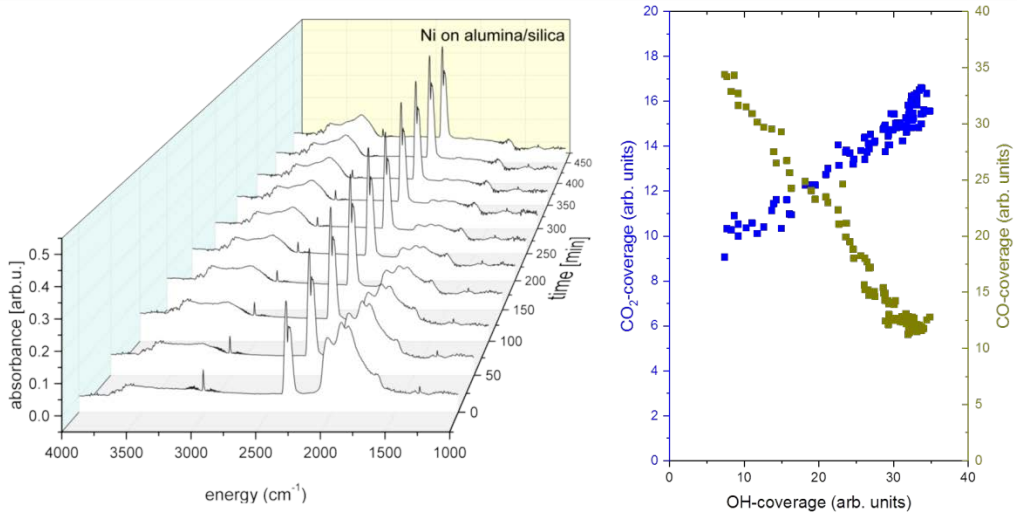

Figure 13: DRIFTS measurement during CO_2 methanation on Ni on silica alumina (without relevant water adsorption).

Long term studies brought to the fore that water accumulates on the surface of the catalyst. This has a detrimental effect on the catalytic activity. While CO_2 adsorption is slightly enhanced, the adsorption of CO and therefore CH_4 reaction rate is strongly reduced (Fig. 13). This effect is the basis of the sorption enhanced methanation: by adding another functionality of the catalyst, the ability of adsorbing large quantities of water, the blocking of active sites is diminished [5]. This functionality and the optimization of the adsorptive support are described in detail in section 4.3.

Here, we highlight the changes of the reaction mechanism induced by water sorption enhancement. The water removal enhances only the reaction steps, during which water is formed, i.e., reaction steps (2d) and (2e). This leads to a higher concentration of carbon at the surface, which is precursor of irreversible soot formation leading to an inactivation of the catalyst, the so-called “coking”. It was thus of high relevance for the project to investigate whether this phenomenon occurs, to what extent, and to develop regeneration procedures. For this, we run long term methanation experiments with different operation times in order to evaluate the carbon concentration possibly formed during operation. Carbon concentrations were determined by exposing the samples to pure oxygen in a tubular oven at 1350°C and measuring the CO_2 emitted by carbon combustion in real time by non-dispersive infrared spectrometry. The carbon content increases roughly by a factor 4 between the as-prepared specimens and the catalysts that have been utilised for catalytic screening (Fig. 14). Classical coking on the surface of the catalytic Ni particles is expected to increase with time as well as temperature [20]. However, the carbon content is neither influenced by the methanation time, nor by the reaction temperature, although the catalytic performance decreases at very high temperatures. It remains at an average of 0.11 ± 0.01 wt.%, i.e., there is no significant carbon uptake by the sorption catalysts during catalysis. Therefore, the results from the performance tests as well as the carbon analysis demonstrate a very robust behaviour of the catalysts, in particular at typical operation temperatures. Apart from water, zeolites adsorb CO_2, CO, and various other carbon containing side products such as carbonates, and higher hydrocarbons. Adsorbed CO_2 could remain in the zeolite pores even at zero CO_2 partial pressure, i.e. also during specimen transport in air between the methanation experiments and melting in the tubular oven, but this amount will not increase with reaction time. Since diffusion of CO_2 in the pores of the zeolite used (LTA 5A) is relatively fast, other adsorbed carbon containing intermediates may contribute to the total carbon content. Again, these compounds will not accumulate during the course of the reaction. With concentrations as low as 0.1 wt.%, the chemical analysis of these compounds is a challenge. DRIFTS can identify most of possible adsorbates on a catalyst surface. These DRIFTS-measurements on Ni-

zeolite showed the reversible coverage by CO, H_2O, and carbonate species [5, 21]. As the latter ones may also be formed on the zeolite surface, the diffusion on them to the catalytic Ni-surfaces may be slightly slower than their formation, and thus accumulate in the zeolites. This hypothesis is underlined by the measurement of the carbon uptake of a cycled sorption catalyst. The sequence consisting of a methanation step of 30 min and a drying step of 1 hour has been repeated 39 times, for a total methanation time of 19.5 hours (Fig. 14). Here, the carbon content is higher than in the specimens that have undergone continuous methanation experiments, even with longer methanation times at the same temperature. During drying, any carbonaceous species is not anymore competitively adsorbed with water, which eases its adsorption in the zeolite, and may block some pores. The correspondingly slower diffusion process was observed and is discussed later (see section 4.2.2, Fig. 18).

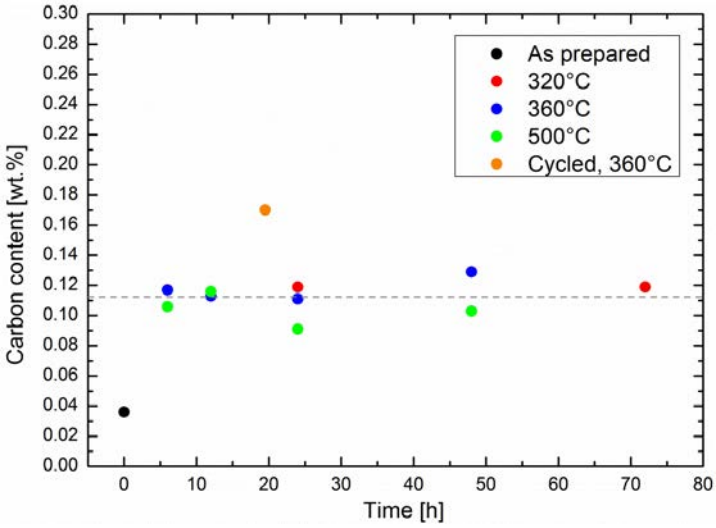

Figure 14: Gravimetric carbon content in Ni-impregnated 5A zeolite specimens subjected to continuous methanation experiments (red, blue and green dots, average of the latter shown by the grey line) and multiple methanation/drying cycles (orange).

The robustness of the sorption catalyst might be explained by the integration of the catalytically active Ni-particles in the support instead to on the support as usual in established Ni-alumina/silica catalysts.

We conducted STEM-tomography to visualize the 3D structure of the catalyst [21]. The tomography demonstrates that Ni-particles agglomerate not only at the outside of the crystals, but also inside the particles (see Fig. 15). A growth of large carbon particles is oppressed inside the particles due to space restrictions.

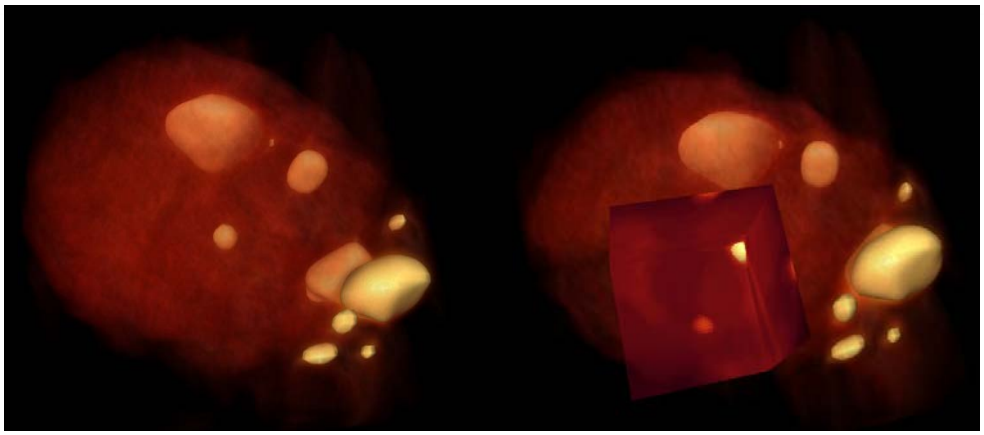

Figure 15: 3D Transmission Electron microscopy image on Ni-zeolite 5A5M. Top micrograph: Visualization of zeolite, and bottom micrograph a Ni particle inside of the zeolite visualized by a corner cut. The image size is around 150 nm x 100 nm. From Ref. [21].

4.2.2 Interplay between catalytic activity and diffusion

One way to see the sorption enhancement of methanation is that the exothermic adsorption of water adds up to the overall reaction heat and thereby reduces the reaction temperature and increases conversion efficiency. This is a thermodynamic argumentation: the free energy of the system defines the reaction path. A realization of a sorption reaction should thus not require peculiar “sorption catalysts” - lowering the water partial pressure by plain physical mixture of catalysts and sorbent should be sufficient to shift the equilibrium of the Sabatier reaction towards the product side as has indeed been demonstrated [22]. However, to have significant influence on the kinetics of the catalytic process, water removal by the adsorbing support must be faster than water formation by the active catalysts. This requires high diffusion coefficient and short diffusion lengths.

Within this project, we optimized the adsorptive properties of the sorption catalysts by comparing the performance parameter (catalytic conversion) of various Nickel impregnated zeolites (3A, 4A, 5A, 13X), and by a careful characterization of the material. A surprising side effect discovered during the investigation of possible degradation phenomena (as described above) is that the macroscopic scale has strong influence on the performance of the sorption catalyst. We thus performed a detailed study of the kinetics on a mesoscopic scale as well macroscopic scale using neutron imaging and neutron microscopy.

For macroscopic measurements, a 200 W model reactor (total volume 750 ml, compare) was placed in a collimated neutron beam at the radiography station NEUTRA 7 [23]. The station is applied to one of the four twin beam lines for thermal neutrons at SINQ, PSI Switzerland. The neutrons are markedly scattered by hydrogens and thus water only, in particular aluminium has a relatively low attenuation cross section for neutrons. Thus, changes of the neutron beam intensity detected through a scintillator plate by a CCD camera are due to differences in the local water content in the reactor (Fig. 16). As we are interested only in the water distribution in the reactor, the pictures are normalized by a reference picture of the dry reactor. Simultaneously, the product gases are led through an FTIR-gas cell. The absorption of the infrared radiation is used to measure the concentration of CO_2 and CH_4. Fig. 16 gives a typical experimental result of the relative neutron absorbance of the reactor bed during reaction and regeneration. Dark regions, i.e., increased neutron absorbance, are regions with higher water content. The water originates from the Sabatier reaction, which is adsorbed by the zeolite, while the methane leaves the reactor. The neutron images show the formation of a reaction front running through the reactor. As the product gas is continuously monitored, we can correlate water content of the sorbent and catalytic activity: there is nearly zero CO_2 leaving the reactor as long as the total water content

increases linearly. With reaching water saturation (the reaction front reaches the end of the catalyst bed), unreacted CO_2 is released. The CO_2-flux is then set to zero, and the regeneration phase of the reactor starts. In contrast to the reaction phase, no reaction front is formed; the reactors dries relatively homogenously (a small gradient from inlet to outlet is nevertheless found).

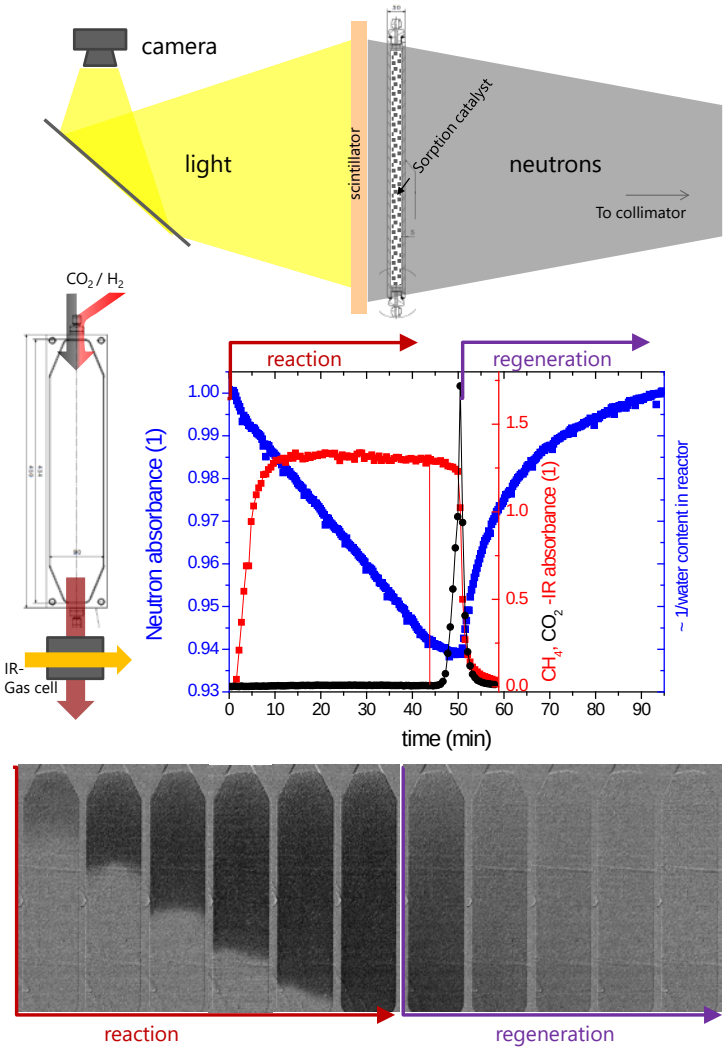

Figure 16: Top: experimental setup used to measure the water content in sorption reactors at the NEUTRA beam line. Middle left: drawing of the reactor with dimensions, and the gas fluxes and gas analysis attached to it. Middle right: experimental data as received from an evaluation of the neutron radiography (changes of neutron absorbance relative to dry reactor in blue) from a time series of pictures (selection shown below) and the corresponding FTIR signal of the CO_2 (black dots) and CH_4 (red dots) leaving the reactor. Hydrogen flux is kept constant, during the reaction and regeneration phase the CO_2 flux is switched on and off, respectively.

The correlations between local water uptake and catalytic performance were further elucidated at three different temperatures 270°C, 300°C, and 320°C. At 270°C, full performance of the catalyst at the used flows (250 ml/min CO_2, 1000 ml/min H_2) is not achieved and a reaction front cannot establish. The catalytic performance does not vary markedly between 300°C and 320°C, here full conversion is reached at both temperatures. The main difference is the water uptake capacity of the sorbent. The maximum water capacity of the zeolite in the reactor at 320°C is only 75% of that in the reactor at 300°C, correspondlingy, the sorption enhanced operation mode stops earlier.

The occurrence of a reaction front is of outmost importance to the functioning of a sorption reactor. A simplified explanation is given in Fig. 17. At the reactor inlet, high conversion of CO_2 into water occurs.

In fact the sorption enhanced mode is only significant, if the yield is determined by thermodynamics, in this case by the products/reactants ratio. In steady state, the water concentration is high at the inlet, and thus limits further conversion. Total conversion is only reached at the reaction front,where the water concetration is low, while still unconverted CO_2 exists. The existence of such a reaction is confirmed by temperature distribution measurements. High conversion rates correspond to high heat evolution resulting in a locally higher temperature. This temperature “peak” runs through the reactor.

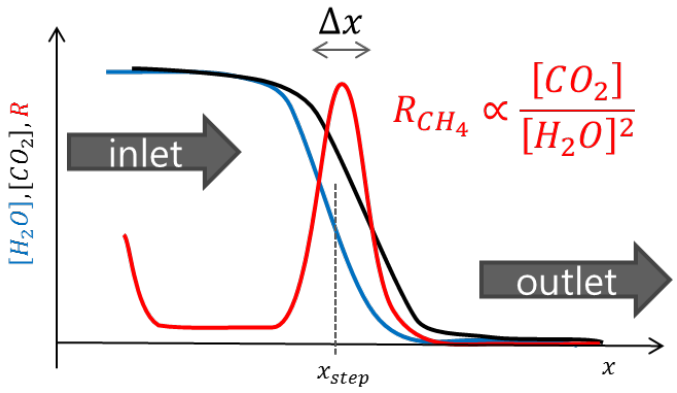

Figure 17: Simplified 1D model of the water and CO_2 concentrations and the corresponding reaction rate (R) around the reaction front (x_{step}) as a function of the position in the reactor (x).

The existence of this reaction front is an advantage for the technical application as a pseudo-continuous methanation reactor. The end of the sorption enhanced mode can be reliably detected and synchronized with the drying mode.

The drying of the reactor represents the rate limiting step in the overall process and emphasizes our approach for a detailed operation process parameter study within this project. While the catalytic performance exceeded the expectations and can be reliably controlled, the drying process is highly non-linear (Fig. 16). Lab-based measurements indicated that the drying process is limited by mesoscopic water diffusion through the catalyst pellets. The mass loss during drying as shown in Fig. 18 can be modelled assuming water diffusion through a sphere of radius $R = 0.075\,cm$ with constant diffusion coefficient of water in zeolites $D = 7.6 \cdot 10^{-8}\,cm^2/s$ at the given measurement temperature:

$$\frac{m_t}{m_{eq}} = 1 - \frac{6}{\pi^2}\sum_{n=1}^{\infty}\frac{1}{n^2}e^{-\frac{Dn^2\pi^2 t}{R^2}} \quad (4)$$

For fitting, the model was further simplified. This is a serious constraint: Obviously, the diffusion model does not depend on gas flow conditions as it is assumes zero water vapor pressure outside the sphere. Finite vapor pressures as a result from insufficient gas flow will further decrease the drying kinetics. This assumption is underlined by the observation from neutron imaging, that hardly any gradient on the macroscopic level is found, indication that each individual pellet has similar desorption kinetics irrespective of the position in the reactor. Furthermore, cycling seems to slightly lower the diffusion coefficient (Fig. 18). This was attributed to a special kind of coking phenomenon (compare previous chapter). From a practical point of view, the results may be simplified by stating that drying times of at least 20 min are needed for obtaining a sufficiently dry sorption catalyst. There are several uncertainties associated with these lab-based measurements, which require additional experiments to underline the critical statement.

With the critical process taking place on the mesoscale, i.e., within one catalysts bead of around 1 mm diameter[1], we were looking for a technique giving insights at this mesoscopic scale. With the good experience from neutron imaging, we utilized neutron microscopy. The physics, and thus evaluation and interpretation of the results from neutron microscopy are similar to the ones described above for neutron images. What is different is specific geometry and setup of the neutron microscope (neutron beamline POLDI) and the reactor setup.

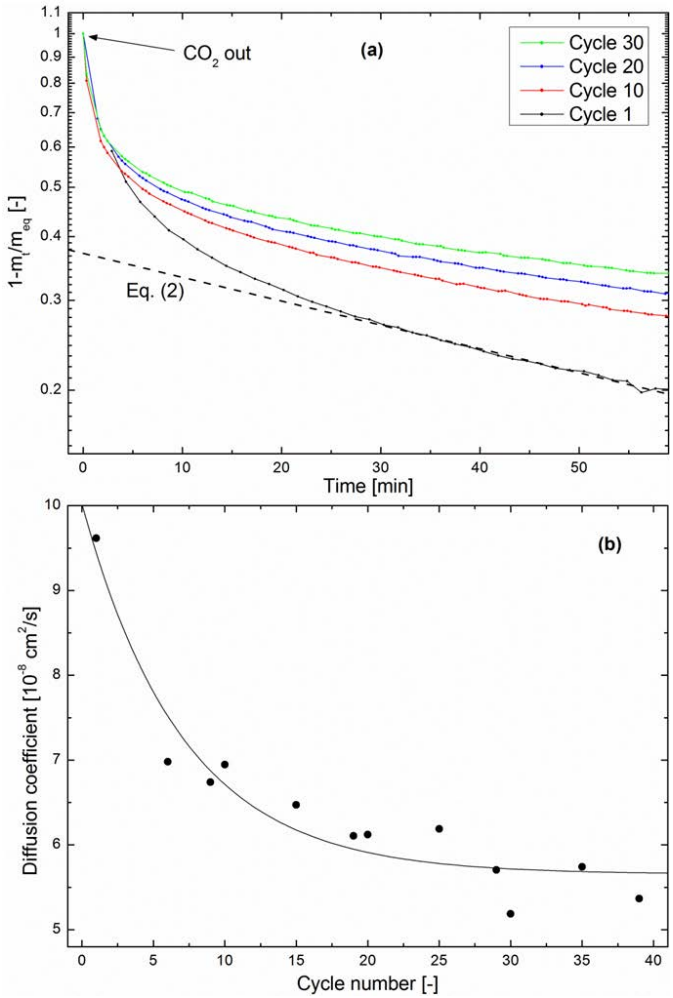

Figure 18: (a) Evolution of the fractional mass loss of a Ni-impregnated 5A zeolite catalyst during drying at 360°C in a multiple cycling experiment. t = 0 s corresponds to CO_2 removal from the system. (b) Diffusion coefficient as a function of cycle number, calculated from fitting Eq. (2) to the late-stage region of drying curves. The solid line is a guide to the eye.

Fig. 19 shows neutron microscopy images of water absorption (top) and desorption (middle) in a sorption catalyst (Ni@13X). The images give interesting insights into the diffusion process of water in porous media. The adsorption of water into the bead is not mirrored by the desorption process. In the first case, a water shell forms at the outside of the sphere and moves inside (so-called moving interface kinetics). A similar, now water depleted shell is not visible for desorption. In addition, a quantitative evaluation yields a much faster adsorption process than desorption process. The qualitative explanation is as follows: The diffusion coefficient of water depends on the total amount of water in the zeolite. During

[1] In most experiments with zeolite 5A, we used pellets, the sorption catalysts based on zeolite 13X with overall better performance are beads of similar size.

adsorption, water diffusion in the outer shell is fast, and the interface with slower diffusion moves inside. During desorption, the outer shell remains the one with the slowest diffusion, as it always has the lowest diffusion coefficient. This leads to a more uniform diffusion with decreasing diffusion coefficient over time. The latter explains also the highly non-linear desorption kinetics (diffusion lengths increases at decreasing diffusion coefficient).

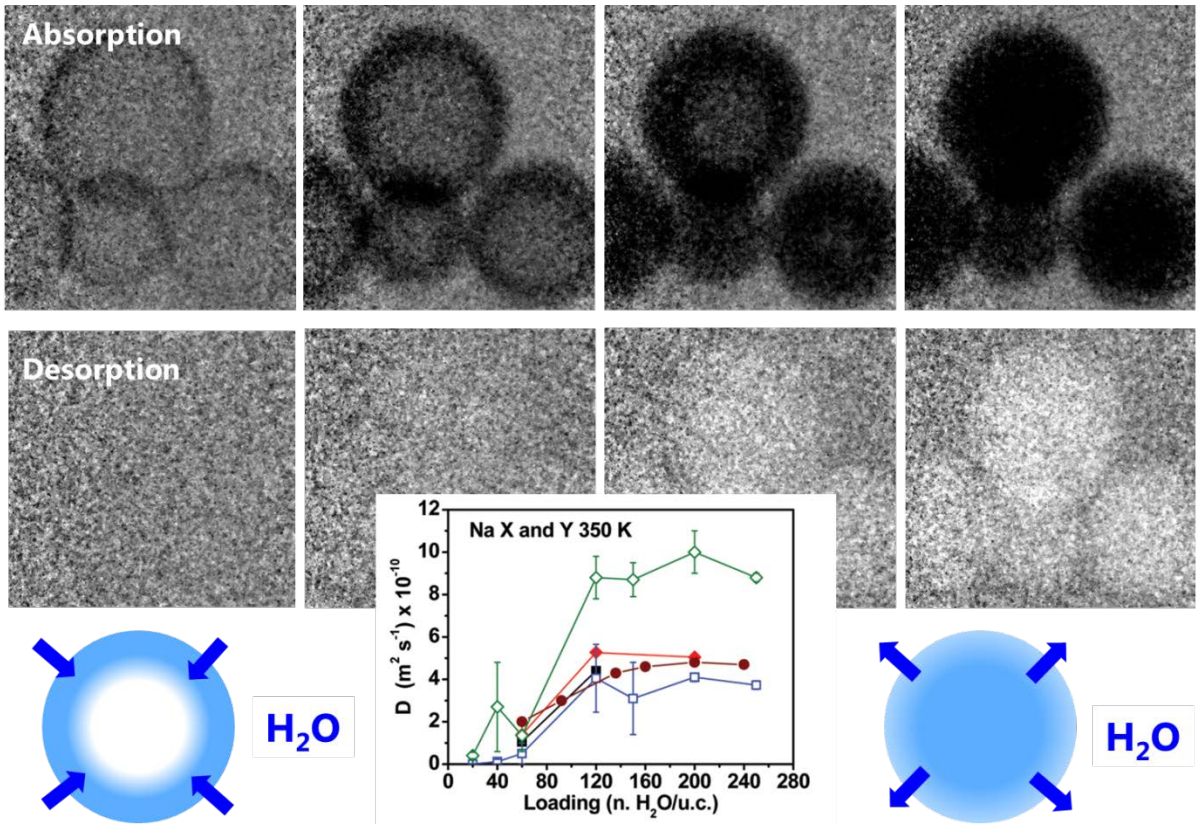

Figure 19: Neutron microscopy images of water absorption (top) and desorption (middle) in a sorption catalyst (Ni@13X) at 100°C. The bottom panels sketch the underlying phenomena: The diffusion coefficient of water depends on the total amount of water in the zeolite, leading to the so-called moving interface model for absorption, and a more uniform but slower diffusion during desorption.

In addition to water sorption kinetics, we measured the water uptake in a single zeolite sphere under methanation conditions. The curves measured on the mesoscopic scale (Fig. 20) are very similar to the one measured for a full reactor (Fig. 16), i.e. the linear water uptake (rate determined by catalytic activity, not diffusion), and highly non-linear desorption. This confirms that indeed the drying kinetics is determined by the kinetics of the individual bead.

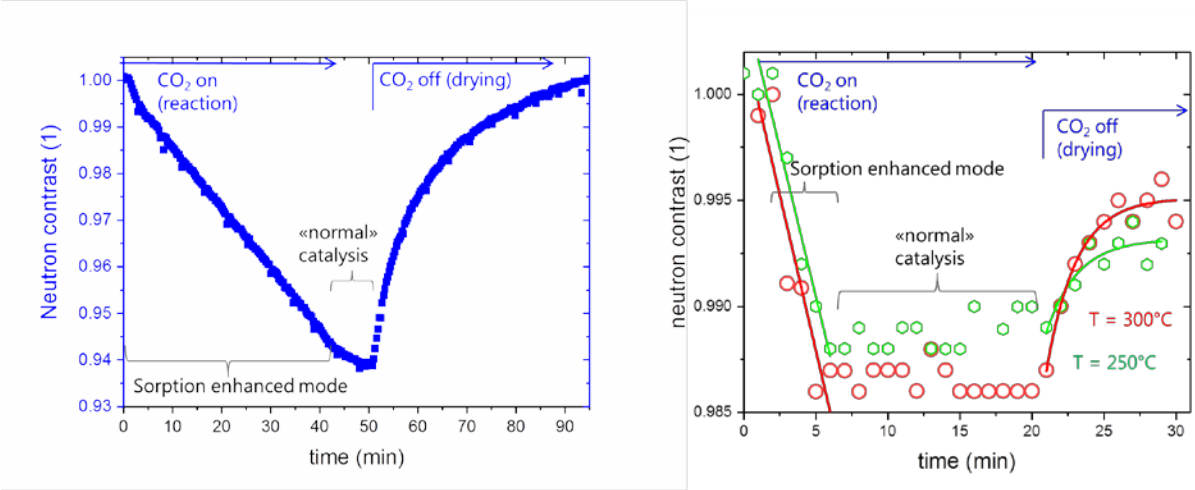

Figure 20: Water uptake of a large scale reactor (left) and of a single catalyst bead during reaction and drying. The time for the sorption enhanced mode can be adapted by the reactor geometry due to the formation of a reaction front, while the regeneration time (drying) is given by the desorption kinetics of the individual bead hardly affected by the reactor dimensions.

4.3 Reactor design

The reactor design is based on the measurements of catalytic performance of the sorption catalyst in addition to the experiences gained from the testing of the 200W model reactor. The considerations are as follows:

The conversion rate of the sorption catalyst can be derived from various experiments probing the catalytic performance $c_{spec} = 0.5 \frac{W}{ml_{cat}}$. The required volume required for a given conversion rate is given by $V[cm^3] = P[W]/c_{spec}[W/cm^3]$. For a reactor with $P = 0.5kW$ we can thus estimate the reactor size to $V_{cat} = 1000ml$ based on the catalytic activity of the sorption catalyst only.

Such a reactor produces water: $n[mol] = \frac{P[kW]}{880kJ/mol} \cdot 2 \cdot t$, where 880kJ/mol is defined by the combustion heat of methane (the chemical energy of the gas produced). However, the formed water can only be absorbed up to the maximum adsorption capacity of the sorption catalyst given by the specific adsorption capacity $\rho[g/cm^3]$:

$$n[mol] = \rho\left[\frac{g}{cm^3}\right] \cdot \frac{V[cm^3]}{18\,g/mol} \quad (5)$$

The maximum capacity is reached at time, after which the sorption enhanced reaction mode does not work anymore:

$$t[s] = \frac{\rho\left[\frac{g}{cm^3}\right] \cdot V[cm^3] \cdot 880\,kJ/mol}{2 \cdot 18\,g/mol \cdot P[kW]} \quad (6)$$

For our 0.5 kW reactor with 1000ml volume, we reach the wet state within 8 min. Here we assumed a specific water capacity at 300°C of 0.01 g/cm^3. Unfortunately, for proper drying, we need 20 min. In a pseudo-continuous operation, we combine two equal reactors in alternating operations, one is producing methane, one is drying. Both modes have to have equal operation times. Therefore, the reactor dimension is given by the drying time, as the running time for sorption enhanced methanation is shorter. Thus we have to run the reactor at a slower pace than given by the catalytic performance of the catalyst. Alternatively, we adapt the reactor size to the drying time needed, i.e. this reactor is slightly bigger:

$$V[cm^3] = t[s]\frac{2 \cdot 18\ g/mol \cdot P[kW]}{\rho\left[\frac{g}{cm^3}\right] \cdot 880\ kJ/mol} = 240 \cdot P[kW] \cdot t[min] \quad (7)$$

For a 1kW reactor we arrive at 2800 ml, i.e. for our 500W plate at a minimum volume of 1400 ml. In addition to the considerations for the total volume, the length, width, and depth may play a role. In pre-experiments using the 200 W reactor having 750 ml, the formation of a reaction mode was found to be well established without indications of slower kinetics at edges. We thus chose similar dimensions, ending up at similar length, but slightly larger width and depth to reach a total volume of 1750 ml. Fig. 21 shows the technical drawing of a 500 W plate as part of 1 kW reactor consisting of 4 plates (two 500W couples).

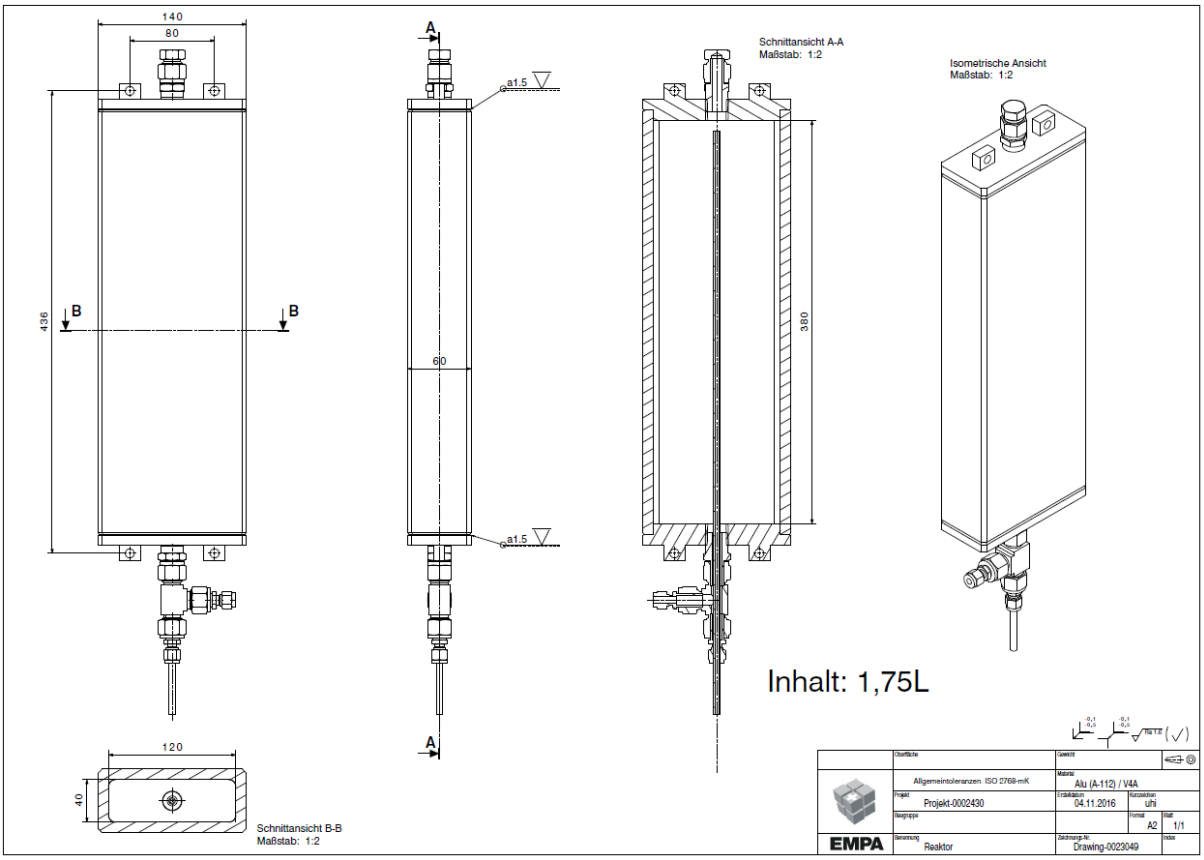

Figure 21: Technical drawing of a 500 W plate for a 1kW reactor stack consisting of 4 plates.

To minimize costs, the construction is based on a commercial cylindrical aluminum profile, which is closed by welded lids on both ends with bores for the gas connections. An important detail is shown in Fig. 22, developed after in-situ temperature distribution measurements during reaction. The gas has to be heated up to the reaction temperature at around 300°C. However, the overall reaction is exothermic, that is, there is enough heat provided by the reaction (once running). Furthermore, the gas has to be cooled down for later use. The solution to this problem is the anti-parallel flux of inlet gas and outlet gas, which works as heat exchanger. The inlet tube reaches the end of the reactor thus avoiding mixing of reactants and products and improves heat distribution in the whole reactor. The heat exchanger idea is of advantage both for reaction and drying mode.

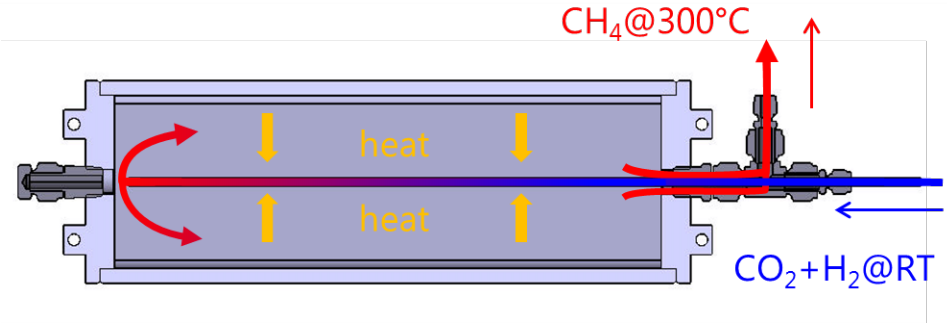

Figure 22: Detail of the gas inlet: the inner tube works as a heat exchanger to pre heat the reactants by heat exchange with the product gas.

The temperature distribution inside a reaction is of high importance, though difficult to address. In a model reactor at ZHAW, the occurrence of a temperature peak running through the reactor following the reaction front was proven as shown by the temperature measurements in Fig. 23. In other words, a "mobile hotspot" is evolving through the reactor towards the outlet, in contrast to other fixed bed applications where the hotspot is immobile. The amplitude of this hotspot is around 60 K.

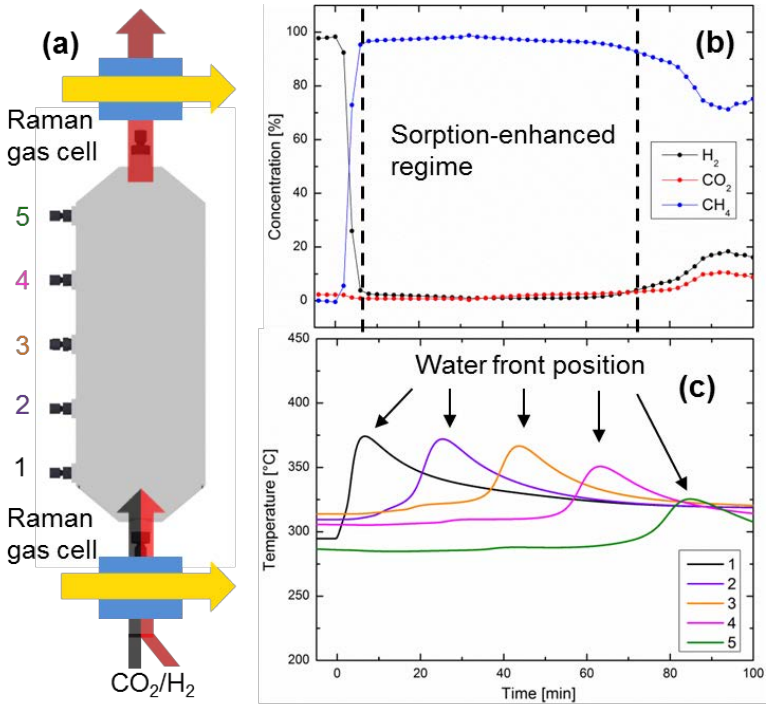

Figure 23: (a) Single plate design with inlet and outlet gas stream in-situ Raman spectroscopy. 5 thermocouples enable vertical temperature resolution. (b) Evolution of concentrations in outlet gas stream as measured by in-situ Raman spectroscopy. (c) Temperature evolution across the reactor length with respect to the evolution of the water front inside the reactor.

However, the exact temperature as well as temperature increase depends on the size and geometry of the reactor and the reaction conditions (averaged reactor temperature, total flow) and external heating and/or cooling. A particular problem of a sorption catalyst is that these catalysts consist of ceramic-like porous media with accordingly very low heat conductivity. Temperature gradients can be relatively large. Within this project, we restricted to estimate the overall heat balance, which is listed in Fig. 24.

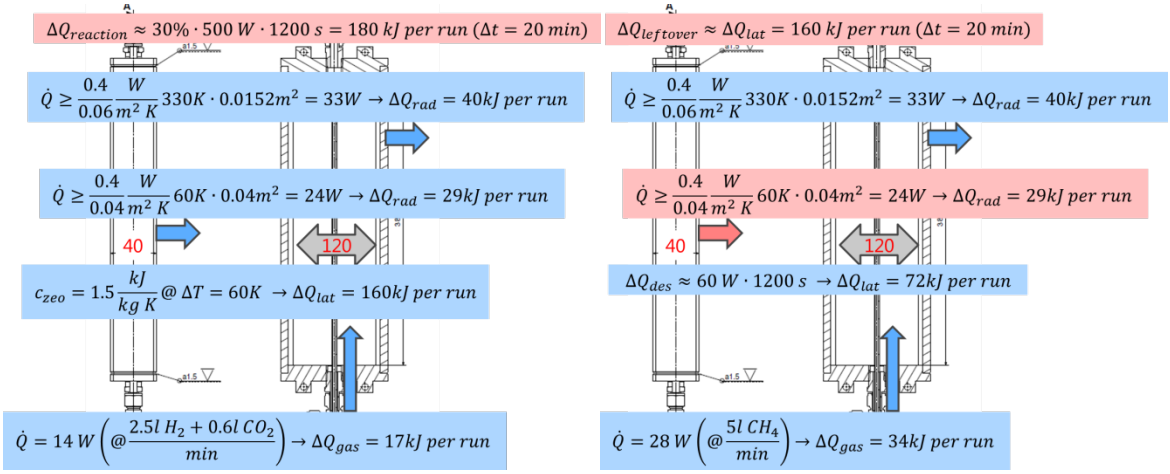

Figure 24: Estimated heat balance of a 1kW sorption reactor, i.e., for one 500W plate in a reactor stack consisting of 4 plates.

Considered terms are:

- Heat of reaction $\Delta Q_{reaction}$ resulting from the Sabatier reaction (-165 kJ/mol) and heat of water adsorption in the zeolite (~-50 kJ/mol). This heat is released during reaction mode.
- Radiation heats from the reactor into environment and to the neighboring reactor ΔQ_{rad}. The first one is a heat loss both for reaction mode and drying mode, while the second term is a heat loss during reaction mode and a heat gain during drying. We assume a temperature difference between reactor and drying mode of 60 K (compare also Fig. 24).
- Latent heat ΔQ_{lat} is the latent heat stored during heating up the sorption catalyst during reaction. This heat is released during drying.
- Latent heat ΔQ_{gas} put into the gas entering the reactor during reaction and drying mode. During reaction mode, the amount of gas cannot be changed as it is defined by the reactor throughput. For drying, the heat flow can be adjusted, and may serve as an easy external temperature control.

The heat balance is given for typical reaction conditions of the 500W reactor. The numbers cancel out within a certain uncertainty. This means that the exact temperature can be controlled externally by adjusting the flow of the drying gas medium and the external heating power.

4.4 Reactor fabrication and test operation

A crucial Milestone in the project was the setting up of a1 kW reactor. This reactor follows the construction drawing in Fig. 21 including non-automatic valves and the catalyst filling (7.5 kg). The amount reached the maximum production capacity of the two involved research institutions (ZHAW and Empa).

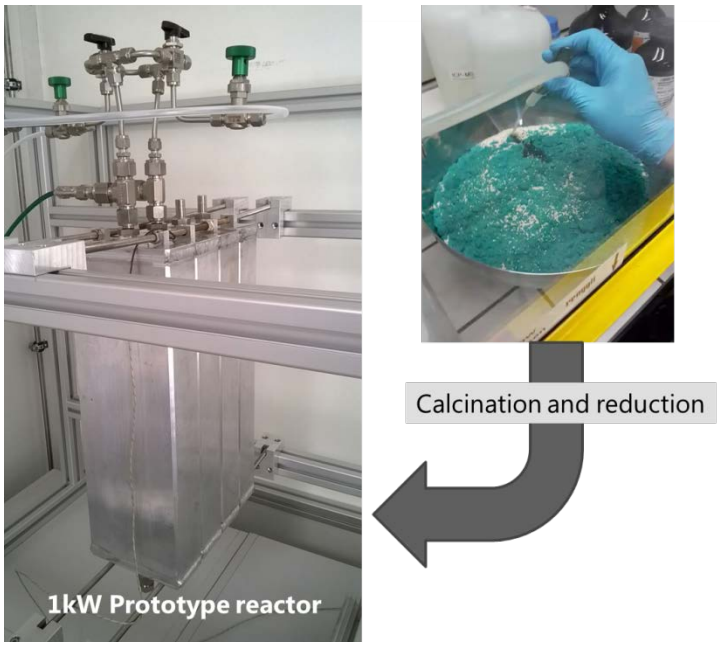

Figure 25: Photograph of the 1kW sorption reactor (left), and a picture during fabrication of the catalyst (right).

5. Conclusion

In the frame of the SMARTCAT project, two novel catalyst functions for CO_2 methanation from biogases were successfully developed: a self-regeneration concept to clean off from typical biogases and a sorption based concept for 100% methane yield. The latter sorption catalysts, as well as the related specific reactor design, were brought to kilowatt scale and the performance upgrade with respect to current systems was demonstrated. The self-regenerating catalyst can be applied in conventional tube reactors, identical to already used technologies.

When operated in **sorption enhanced** conditions - i.e. as long as the water-affine support is not saturated at the optimal operation temperature of 300°C - the catalyst itself delivers an outstanding CO_2 conversion of 100%. No side products were observed, meaning that the methane yield is also 100%. This is a highly valuable result with respect to the economic efficiency of the process, notably because biogas mixtures can be upgraded towards their full energetic potential with the help of such technology, and because dry methane is provided, without requirement of gas separation. Additionally, we improved the catalyst performance in terms of catalyst-support interaction. Optimisation of the relevant operation parameters - temperature, pore size, bead size, water adsorption capacity, regeneration gas - allow for maximisation of the sorption enhanced methanation time and effective catalyst regeneration. A novel reactor concept adapted to this particular process was developed in parallel. The fact that the reactor scales with water production by the Sabatier reaction makes this process unique. We solved this problematic by designing a modular reactor concept, taking into consideration crucial parameters like the kinetics of water evolution through fixed-bed reactor plates, the synchronisation of methanation and drying kinetics and the heat transfer between reactor modules. Long-term catalyst operation was also addressed, with encouraging outcome with respect to coking and microstructural deactivation, which turned out to be practically inexistent. The most problematic obstacle with respect to biogas upgrade is sulfur poisoning, which is known for Ni-based catalysts. Here, it is recommended to separate sulfurous species prior to conversion. However, in terms of materials development, the potential of sorption enhanced methanation remains important. We aim at studying new active elements and alloys, among others, in order to tackle the problematic of sulfur poisoning and reduce the catalyst production costs. As a final perspective for this technology, reactor upscale beyond kilowatt scale was recently initiated, with the goal of integrating sorption enhanced methanation in a biogas based PtG plant.

Secondly, redox-triggered **self-regeneration of smart catalysts** was studied at a material level. Perovskite-based materials were developed with a particular focus on matching the redox conditions to the operation conditions for CO_2 methanation. We provided an experimental proof of the self-regeneration concept for LNF-type perovskites, while at the same time, we showed that the activity of such catalysts competes with commercial materials. Furthermore, these catalysts contain much less Ni (factor two or even beyond) compared to commercial counterparts. The optimal operation temperature is in the range of 450 - 500°C, which fits well with the Ni exsolution conditions which are at least at 400°C in H_2. The reincorporation by an oxidation step is more demanding. Temperatures of at least 600°C are required for activation of Ni reincorporation. Technologically speaking, regular catalyst regeneration in such conditions is feasible. Moreover, long-term catalyst operation and multiple redox-cycling demonstrated the excellent robustness of this material. Here again, sulfur poisoning is the most critical obstacle to industrialisation. It seems to impede Ni reincorporation into the perovskite host matrix, forcing to readjust to harsher oxidation conditions. Here again, a typical weakness of Ni catalysts is reflected in our technology, but this is not a fatality. We are currently studying the possibility of reproducing the self-regeneration concept with other active elements/alloys to enhance sulfur tolerance. Regarding technology scale-up, we are currently studying different methods for handling of the nanopowders at a larger scale.